Classical, first order, and advanced theories

Michele d'Ottavio, Olivier Polit

Classical, First order and Advanced theories

M. D'Ottavio and O. Polit*

UPL, Univ Paris Nanterre
Laboratoire Energétique, Mécanique, Electromagnétisme
50 rue de Sèvres - 92410 Ville d'Avray - France

Abstract

This chapter is dedicated to theories for the mechanical analysis of structures. An overview of the literature is given based on classical and advanced theories. A general classification is first introduced concerning displacement or mixed models, asymptotic or axiomatic approaches and Equivalent Single Layer or Layer-Wise modeling techniques. The proposed classification pertains to beam, plate and shell models. Classical theories and advanced ones are subsequently presented with precise description of the underlying hypotheses. For the sake of conciseness, the mathematical description is limited to plate structures and beam theories are briefly discussed in the Appendix. Some numerical results are given for layered and sandwich structures with respect to linear bending, free vibration and buckling analyses. The model assessment allows to define applicability ranges and limitations of these theories.

Keywords: Theories, Models, Beams, Plates, Shells, Laminates, Sandwich structures, Benchmarks

*olivier.polit@u-paris10.fr

Contents

1. Introduction and classification

Laminated and sandwich structures. Composite structures allow to optimize the design of mechanical components by offering the possibility of tailoring the distribution of materials with different mechanical properties inside the loading paths. Two major classes of composite structures can be identified: Composite *laminated structures* are formed by stacking plies made out of a composite material with a specific fiber orientation; *Sandwich structures* classically consist of a core made of a rather bulk, light-weight and compliant material that is "sandwiched" between two rather thin but stiff faces or "skins", that may be composite laminates. The main property of sandwich structures is their enhanced specific bending stiffness. A perfect bond between the different materials composing the composite structure avoids interfacial slips and assures the continuity of the loading path. Throughout this chapter, composite structures are thus considered as a perfectly bonded stack of homogenous, anisotropic materials.

Beam, plate and shell models. Any structure is a three-dimensional solid, whose behavior is mathematically described by three-dimensional governing equations for the problem to be considered, that include field equations as well as boundary and initial conditions. Since the solution of the three-dimensional problem is in general a cumbersome task, a reduced model is often invoked for representing the functional response of the structure. These *structural models* are essentially suggested based on the geometry of the considered structure; the behavior along directions whose geometric dimensions are small compared to others is hereby no longer resolved within the three-dimensional equations, but it is instead represented in a simplified manner. So, *shell models* are formulated for structures having one dimension (the thickness) much smaller than two in-plane dimensions characterizing the reference surface: the response across the thickness direction is then reproduced by means of a simplified model whose parameters are taken to vary along the two directions defining the reference surface. Shell models are therefore two-dimensional models. In an analogous manner, *beam models* are formulated upon describing in a simplified manner the response within the cross-section, whose dimensions are much smaller than the length of the segment perpendicular to it representing the beam axis. The behavior of the cross-section is then defined by parameters that are taken to vary only along the beam axis, i.e., a one-dimensional model is considered. If the shell's reference surface has no curvature, the shell model degenerates to a *plate model*. In general, a curved structure is characterized by a ratio between length and radius, which defines its "deepness" or "shallowness", see Fig. 1. In the literature, models

could be classified as shallow or deep shell models with respect to this ratio, introducing simplifications on the curvature radius in the strain expressions [1]. In particular, a shallow shell could be considered "like a plate" as far as the transverse shear strain components are concerned.

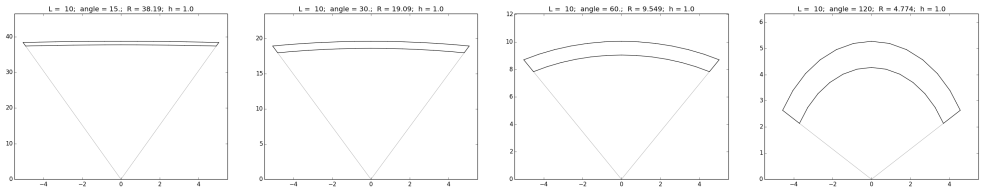

Figure 1: Geometry of curved beams of constant span-to-thickness ratio L/h: from shallow to deep.

The pertinence of a structural model can be defined by its capability of capturing with a satisfying accuracy the relevant mechanical response of the real three-dimensional structure. One may identify a membrane, bending and torsion or twisting response, depending on the loading path of the structure, which is in turn determined by geometric considerations and constitutive behaviors. Moreover, the critical design criteria may be related to stiffness or strength: the relevant response may be, in the first case, a displacement or a frequency, in the second case a strain or stress. Therefore, the *accuracy* of structural models, that is, their capability to correctly reproduce the three-dimensional behavior, depends not only on the geometric ratios of the actual structure, but also on the wavelength of the response to be investigated. This consideration yields two important conclusions; on the one hand, it is clear that the model accuracy depends on the considered problem, in particular on the loading conditions and which is the mechanical response of interest (displacement or stress, a fundamental or high frequency); on the other hand, it may be anticipated that, in comparison to homogeneous structures, the response's wavelength along the stacking direction of composite structures is shorter due to the material discontinuity.

Asymptotic or axiomatic approaches. Two main approaches have been proposed to derive structural models from the three-dimensional elasticity theory. The *axiomatic approach* consists in postulating the simplified behavior, the "*a priori* assumptions", on the basis of empirical evidence or mechanical insight about the functional response of interest. For instance, Leonardo da Vinci early observed that cross sections of a straight beam in pure bending remain plane and perpendicular to the beam axis [2]; this observation

permits to postulate some kinematical hypotheses that simplify the three-dimensional equations. As a further example, it may be *reasonably assumed* that the out-of-plane normal stress within a thin plate be negligibly small compared to the primary bending stresses [3]. This assumption allows to formulate some simplifying hypotheses concerning the static response.

Despite this approach has been widely employed over the last centuries, it cannot in general provide a mathematically sound relationship with respect to the three-dimensional behavior. In other words, it is not possible to provide a measure of the error introduced by the simplifying hypotheses and, therefore, to define the range of applicability of the simplified model.

The *asymptotic approach* can be seen as a step towards the resolution of this drawback. In this approach, the three-dimensional behavior is described mathematically as a series expansion in terms a dimensionless "small parameter" δ that contains the physical characteristics of the structure considered for the model reduction. In curved beam and shell structures, this parameter is often defined as the ratio between the thickness and the curvature radius, in straight beams and plates as the ratio between the thickness and the span. The reduced model is then constructed upon truncating the resulting system of equations up to a predefined order of the parameter. This way, successive approximations are possible, which allows to introduce higher-order terms (in the asymptotic sense) that have a controlled contribution to the structural behavior. Moreover, the derived model exactly recovers the three-dimensional solution for $\delta \to 0$. The works by Gol'denveizer [4, 5] and Cicala [6] can be mentioned for referring to comprehensive examples for this approach to homogeneous plates and shells. An asymptotic approach to beam structures can be found in [7]. While the aforementioned "formal" asymptotic approach manipulates directly the three-dimensional differential equations, an alternative method introduces asymptotic expansions within variational forms, see, e.g., [8]. This latter method has certain advantages, in particular with respect to its application to composite structures and anisotropic materials, see, e.g., [9, 10]. It is worthwhile noticing that the classical plate model formulated by Kirchhoff through *a priori* assumptions could be mathematically justified by means of the asymptotic approach [11].

Displacement or mixed models. In the framework of the most widespread axiomatic approach, once the simplified field distributions have been formulated, the structural model is derived by referring to variational formulations, in particular energy principles or, more generally, virtual work principles [12]. So, the principle of minimum of potential energy, or principle of virtual displacements (PVD), is invoked in conjunction with an assumed displacement field (kinematic assumptions), whereas the principle of minimum comple-

mentary energy is invoked along with an assumed stress field (static assumptions). The former case leads to a so-called displacement-based model, the latter case to a stress-based model. In order to enhance the model's accuracy, mixed approaches have been proposed that allow to introduce simultaneously approximations for both, the displacement and the stress fields [13]. Reissner proposed a mixed variational principle expressly dedicated to composite structures, in which independent approximations can be introduced for the displacement field and the *transverse* stresses acting along the stacking direction [14]. This way, the transverse stress field can be chosen so to exactly fulfill the equilibrium between plies as well as at the outer surfaces of the structure by an exact balance with the applied loads [15].

ESL or LW developments. The formulation of axiomatic models for composite structures requires to select whether the simplifying assumptions are introduced for the whole materials' stack or for different constituting layers independently. The former case amounts to a direct application of the classical axiomatic approaches, early developed for homogeneous structures, to the heterogeneous composite stack. The behavior of the structural model is here defined by unknown functions that vary along one given reference line (at a given point of the cross-section) for beams, or along a given reference surface (at a given height across the thickness) for shells/plates. This kind of description is usually referred to as *Equivalent Single Layer (ESL)* for it homogenizes the composite stack to one single material layer, whose properties are evaluated from the material constants and geometry of the individual plies. In ESL models, the number of unknown functions is thus independent from the actual number of plies constituting the composite structure and it depends only on the order of the approximation that is introduced. A different approach consists in introducing the approximations independently for all individual plies constituting the composite stack; the individual layer models are subsequently assembled for satisfying the interlaminar continuities that reproduce the perfect bond conditions. This so-called *Layer-Wise (LW)* description allows an explicit representation of the individual stiffnesses of the plies and of their interfaces, but the number of unknown functions describing the structural model does depend on the number of layers that have been separately modeled. Alternatively, still starting from independent approximations in separate layers, the interlaminar continuity conditions can be exploited so to eliminate the layer-specific unknown functions and thus recovering a structural model whose number of unknown functions is independent from the actual number of layers: this class of models is generally referred to as *Zig-Zag models*. The authors refer to the historical note [16] for a comprehensive discussion about Zig-Zag models.

Numerical methods and errors. Once the structural model derived, the solution is sought in a reduced dimensional space, i.e., in one dimension for a beam model and in two dimensions for a shell/plate model. An exact solution, that verifies in strong form all equations of the boundary value problem, can be found for some simple academic cases. If an exact three-dimensional elasticity solution is also available, these simple case studies are valuable for they allow to numerically assess the accuracy of the structural model itself. In most cases, however, no exact solution can be found and it is necessary to resort to approximate, numerical solution methods. In the framework of the finite difference method, the governing equations of the boundary value problem are discretized, and subsequently solved in strong form. An alternative and more powerful approach is to look for weak form solutions, i.e., approximate solutions that satisfy in "some sense" the original boundary value problem upon minimizing in a weighted manner their residual with respect to the exact solution. The Finite Element Method (FEM) is by far the most widespread representative for these weighted residual methods [17]. In either case, these numerical solutions come in general with a discretization error in addition to the modeling error.

2. Preliminaries

The main focus of this chapter is on composite plate and beam models, for which the intrinsic parameters driving the model's accuracy will be essentially the thickness (plates) or the cross-section geometry (beams), and the material properties. As mentioned in the Introduction, shell models will require to consider the effect of curvature as well. Classical and advanced plate models will be formulated within the axiomatic approach upon introducing *a priori* assumptions for the displacement field. This preliminary section introduces the fundamental quantities describing the behavior of a three-dimensional composite structure along with the notation that shall be employed throughout the Chapter. Furthermore, it presents the general path to be followed for deriving the axiomatic displacement-based models, which holds for both the classical and advanced theories. The proposed notation will be directly particularized to beam models in Appendix A.

A Cartesian reference frame $(O, \vec{x}_1, \vec{x}_2, \vec{x}_3)$ is introduced for the mathematical description of the structure. Let the composite plate be composed of N_p plies and occupy the volume $V = \Omega \times \left[\frac{-h}{2}, \frac{h}{2}\right]$, where Ω is the reference surface in the (x_1, x_2)-plane and $h = \sum_{p=1}^{N_p} h^{(p)}$ is the thickness measured along the x_3 coordinate. The thickness is taken to be constant over Ω. The plate's boundary $\partial V = \Gamma = \Gamma_{\text{lat}} \cup \Gamma_{\pm}$ is composed of $\Gamma_{\text{lat}} = \partial\Omega \times \left]\frac{-h}{2}, \frac{h}{2}\right[$ and

$\Gamma_{\pm} = \Omega \times \left\{\frac{-h}{2}, \frac{h}{2}\right\}$. Further, let the boundary be subjected to geometric constraints (imposed displacements) on the portion Γ_u and to static constraints (imposed surface loading) on Γ_t, with $\Gamma_u \cup \Gamma_t = \Gamma$ and $\Gamma_u \cap \Gamma_t = \emptyset$.

2.1. Strain, stress and constitutive relation

At any time instant t and in any point of the solid structure, the stress and strain fields are defined by the second-order tensors $\sigma_{ij}(x_1, x_2, x_3; t)$ and $\epsilon_{ij}(x_1, x_2, x_3; t)$, respectively, with $i, j \in \{1, 2, 3\}$ corresponding to the three orthogonal directions x_i of the Cartesian reference frame. Throughout this chapter reference is made to infinitesimal deformations, the following geometrical relations are thus supposed to hold between the strain components and the displacement field $u_i(x_1, x_2, x_3; t)$:

$$\epsilon_{ij} = \frac{1}{2}\left(u_{i,_j} + u_{j,_i}\right) \tag{1}$$

where the notation $u_{i,_j}$ indicates the partial derivative of the component u_i with respect to the x_j direction. By virtue of the symmetry of the stress and strain tensors, the compact Voigt-Kelvin notation is adopted according to

$$\sigma_1 = \sigma_{11};\ \sigma_2 = \sigma_{22};\ \sigma_3 = \sigma_{33};\quad \sigma_4 = \sigma_{23};\ \sigma_5 = \sigma_{13};\ \sigma_6 = \sigma_{12} \tag{2}$$

$$\epsilon_1 = \epsilon_{11};\ \epsilon_2 = \epsilon_{22};\ \epsilon_3 = \epsilon_{33};\quad \epsilon_4 = \gamma_{23};\ \epsilon_5 = \gamma_{13};\ \epsilon_6 = \gamma_{12} \tag{3}$$

with $\gamma_{ij} = 2\epsilon_{ij}$ $(i \neq j)$ denoting the engineering shear strains. The constitutive link between the strain and the stress fields depends on the material properties of the ply (p) and is expressed for linear elasticity by the generalized Hooke's law

$$\sigma_{ij}^{(p)} = C_{ijkl}^{(p)}\epsilon_{kl}\ \ (i, j, k, l \in \{1, 2, 3\}) \quad \text{or} \quad \sigma_p^{(p)} = C_{pq}^{(p)}\epsilon_q\ \ (p, q \in \{1, 2 \ldots 6\}) \tag{4}$$

where the last expression employs the compact notation according to which $C_{pq}^{(p)}$ is the 6-by-6 matrix of elastic stiffness coefficients of the material constituting the ply (p). A composite material ply is described as a homogeneous medium with orthotropic symmetry in its principal material axes X_i, where X_1 is the fiber direction and X_2 and X_3 the transverse directions. Limiting the attention to constant stiffness composite materials, for which the fiber direction X_1 is independent from the spatial coordinates, the orientation of the fibers of each ply is defined by a rotation angle $\theta^{(p)}$ about the transverse direction X_3. According to this transformation, the composite material will possess a monoclinic symmetry in the structural reference frame x_i, and the

rotated elastic stiffness matrix $C_{pq}^{(p)}$ will have the following general form:

$$C_{pq}^{(p)} = \begin{bmatrix} C_{11}^{(p)} & C_{12}^{(p)} & C_{13}^{(p)} & 0 & 0 & C_{16}^{(p)} \\ & C_{22}^{(p)} & C_{23}^{(p)} & 0 & 0 & C_{26}^{(p)} \\ & & C_{33}^{(p)} & 0 & 0 & C_{36}^{(p)} \\ & & & C_{44}^{(p)} & C_{45}^{(p)} & 0 \\ & \text{sym} & & & C_{55}^{(p)} & 0 \\ & & & & & C_{66}^{(p)} \end{bmatrix} \tag{5}$$

2.2. Construction of the two-dimensional model

According to the displacement-based axiomatic approach, *a priori* assumptions are introduced for the displacement field upon making explicit its dependence along the thickness direction $x_3 = z$. The assumptions may thus be formally written as

$$u_i(x_1, x_2, z; t) = F_{s_i}(z)\tilde{u}_{s_i}(x_1, x_2; t) \qquad \text{with } s_i = 0, 1, 2, \dots N_i \tag{6}$$

where the N_i functions $F_{s_i}(z)$ contain the kinematic assumptions for the displacement component u_i. Note that Einstein summation convention over repeated indexes is employed. A powerful means for constructing the dimensionally reduced model makes use of integral expressions related to physically sound variational formulations [17]. The Principle of Virtual Displacements extended to dynamics problems is Hamilton's principle:

$$\int_{t_1}^{t_2} \left\{ \int_V \rho \frac{\partial^2 u_i}{\partial t^2} \, \delta u_i \, \mathrm{d}V \; - \int_V b_i \, \delta u_i - \sigma_{ij} \, \delta \epsilon_{ij} \, \mathrm{d}V + \int_{\Gamma_t} t_i \, \delta u_i \, \mathrm{d}\Gamma \right\} \, \mathrm{d}t = 0 \tag{7}$$

where ρ is the specific mass, while b_i and t_i are the body forces in V and imposed tractions on Γ_t, respectively. The symbol δ denotes the virtual operator, which for Hamilton's principle acts on an *admissible* displacement field, i.e., the virtual variations of the assumed displacement field are required to verify the geometric strain-displacement relations Eq. (1) as well as

$$\delta u(x_i, t) = 0 \qquad \forall x_i \in \Gamma_u, t \in [t_1, t_2] \quad \text{and} \quad \forall x_i \in V, t \in \{t_1, t_2\} \tag{8}$$

The analysis shall be further restricted to hyperelastic materials, for which Eq. (4) holds throughout the dynamic deformation: substitution of Eq. (4)

and Eq. (1) into Eq. (7) yields

$$\int_{t_1}^{t_2} \left\{ \int_V \rho \, \frac{\partial^2 u_i}{\partial t^2} \, \delta u_i \, \mathrm{d}V \right. \\ - \int_V b_i \, \delta u_i - \frac{1}{4} C_{ijkl} \left(\frac{\partial u_k}{\partial x_l} + \frac{\partial u_l}{\partial x_k} \right) \left(\frac{\partial \delta u_i}{\partial x_j} + \frac{\partial \delta u_j}{\partial x_i} \right) \mathrm{d}V \\ \left. + \int_{\Gamma_t} t_i \, \delta u_i \, \mathrm{d}\Gamma \right\} \, \mathrm{d}t = 0 \quad (9)$$

where the sum is implied over $i, j, k, l \in \{1, 2, 3\}$.

The two-dimensional reduced model is thus obtained upon introducing the assumption Eq. (6) into Eq. (9) and carrying out explicitly all differentiations and integrations with respect to the coordinate z. The integration over the thickness h is hereby split over the N_p ply thicknesses to account for the ply-specific material properties, viz.

$$\int_V (\ldots) \mathrm{d}V = \int_\Omega \left[\int_h (\ldots) \mathrm{d}z \right] \mathrm{d}x_1 \mathrm{d}x_2 = \int_\Omega \left[\sum_{p=1}^{N_p} \int_{h^{(p)}} (\ldots) \mathrm{d}z \right] \mathrm{d}x_1 \mathrm{d}x_2 \quad (10)$$

The Euler-Lagrange equations of Hamilton's principle, i.e., the conditions to be verified for satisfying the integral statement in Eq. (7) for any virtual variation of the admissible displacement field, correspond to the dynamic equilibrium equations of the body and the equilibrium with the imposed tractions on Γ_t. Once the coordinate z eliminated by the integration over the thickness h of the plate, the governing equations are hence the variationally consistent equilibrium equations defined over the two-dimensional domain Ω.

2.3. Solution methods for the two-dimensional model

Approximate solution methods, such as Ritz method or FEM, introduce approximating "shape" functions $\mathcal{N}(x_1, x_2)$ over the two-dimensional domain Ω for each term of the displacement assumption Eq. (6):

$$\delta \tilde{u}_{r_i}(x_1, x_2; t) = \sum_{m_{r_i}=1}^{M_{r_i}} \mathcal{N}_{m_{r_i}}(x_1, x_2) \, \delta U_{m_{r_i}}(t) \quad (11a)$$

$$\tilde{u}_{s_j}(x_1, x_2; t) = \sum_{n_{s_j}=1}^{M_{s_j}} \mathcal{N}_{n_{s_j}}(x_1, x_2) U_{n_{s_j}}(t) \quad (11b)$$

where $r_i = 0, 1 \ldots N_i$ and $s_j = 0, 1 \ldots N_j$ with $i, j = 1, 2, 3$. Each unknown function $\tilde{u}_{s_j}(x_1, x_2; t)$ is thus expressed in terms of M_{s_j} degrees of freedom

(DOF). Eq. (11) are directly introduced into the integral form of the equilibrium equations as they arise from the two-dimensional variational statement. All spatial derivations and integrations over the two-dimensional domain Ω are subsequently carried out explicitly, which eventually leads to the discrete system of Ordinary Differential Equations in time of the following form:

$$\delta U_m : \quad M_{mn}\ddot{U}_n(t) + K_{mn}U_n(t) = F_m(t) \quad (m, n = 1 \dots M) \tag{12}$$

where M_{mn} and K_{mn} are the mass and stiffness matrix, respectively, which are square and symmetric. The size of the system is $M \times M$, where M is the sum of all DOF used to represent the complete displacement field, viz.

$$M = \sum_{i=1}^{3} \sum_{s_j=0}^{N_j} M_{s_j} \tag{13}$$

The solution of the dynamic problem is generally found by means of numerical time-integration algorithms, such implicit or explicit Euler methods [18]. A free-vibration problem is obtained from the above expression upon assuming a harmonic response $U_n(t) = U_n\, e^{i\omega t}$ and setting the external force to zero: $F_m = 0$, which yields

$$\left[K_{mn} - \omega^2 M_{mn}\right] U_n = 0 \tag{14}$$

Research for a non-trivial solution leads to the solution of the eigenvalue problem

$$\det\left[K_{mn} - \omega^2 M_{mn}\right] = 0 \tag{15}$$

which determines the M eigenfrequencies $f = 2\pi\omega$ and the associated M vibration modes defined by the corresponding eigenvectors.

For an exact solution of the dimensionally reduced plate problem, the two-dimensional integral statement of the variational equation is first manipulated for deriving the strong form of the governing equations, i.e., the equilibrium equations and the static boundary conditions. An exact solution is thus sought for the differential equation systems (two-dimensional Partial Differential Equations in space and Ordinary Differential Equation in time). The Navier-type solution employed on some numerical results of Section 7, is a strong-form solution based on trigonometric functions over Ω that holds for square, orthotropic composite stacks with simply-support boundary conditions at its four edges.

2.4. Bifurcation buckling

Bifurcation buckling is studied as the research of an adjacent configuration a body arrives at upon a small perturbation from an initially stressed

state [12]. The incremental elasticity problem is formulated in terms of incremental Trefftz stress measures, Green-Lagrange finite strain measures and constant elasticity moduli [19]. The attention is limited to the lateral (out-of-plane) buckling of in-plane compressed plates, and a linearization is performed upon assuming that the plate remains flat (undeformed) at the initially stressed state. The variational statement for this linearized stability analysis reads

$$\int_V \delta\epsilon_{ij}\, C_{ijkl}\epsilon_{kl} + (\delta u_{i,\alpha})\, \lambda\sigma^0_{\alpha\beta} u_{i,\beta}\ \mathrm{d}V = 0 \tag{16}$$

The critical load is thus given by the scalar parameter λ that multiplies the initial in-plane stress state $\sigma^0_{\alpha\beta}$ $(\alpha, \beta \in \{1, 2\})$ and for which a non-trivial adjacent equilibrium condition exists. The initial stress is seen to be energetically conjugate to the non-linear term of the in-plane, finite Green-Lagrange strains:

$$\delta u_{i,\alpha}\, u_{i,\beta} = \delta\left(\frac{1}{2} u_{i,\alpha} u_{i,\beta}\right) \tag{17}$$

In conjunction with slender structures such as beams or shells/plates, the non-linear strains defined in Eq. (17) are often simplified according to von Kàrmàn assumption of large rotations and small strains as follows:

$$\delta u_{i,\alpha}\, u_{i,\beta} \approx \delta u_{3,\alpha}\, u_{3,\beta} \tag{18}$$

The two-dimensional plate model is again obtained upon assuming the dependence upon the thickness coordinate $x_3 = z$ through the displacement approximations Eq. (6), and subsequently carrying out explicitly all derivatives and integrations with respect to z. More details can be found in [20], where the equations for the linearized buckling analysis are formulated and solved within a three-dimensional elasticity framework as well as following the approximate plate model approach. As a result, the following linear eigenvalue problem is obtained from Eq. (16) in terms of discrete DOF:

$$\det\left[K_{mn} + \lambda K^{\sigma}_{mn}\right] = 0 \tag{19}$$

where K_{mn} is the linear stiffness matrix issued from the first term in Eq. (16) and K^{σ}_{mn} is the geometric stiffness matrix associated to the initial stress field. The eigenvalues correspond to the critical load of the plate, the lowest of which is the buckling load. The eigenmode associated to the lowest eigenvalue corresponds to the buckling mode.

Some final comments follow. First, it is worth emphasizing that the linearization of the bifurcation buckling analysis neglects the membrane-bending coupling of anisotropic laminates for it supposes the out-of-plane

deflection of the initially stressed configuration to be nil. As a consequence, some conditions on the in-plane loading and edge conditions should be verified for permitting a linear bifurcation buckling analysis of general anisotropic plates [21]. Second, contrary to laminated plates, instability of compressed sandwich plates can involve the whole sandwich plate (global buckling), mainly the core (shear crimping) or mainly the skins (dimpling and wrinkling) [22]. The nature of the buckling response of sandwich structures depends on both, the gross panel's dimensions and the geometric and material ratios between skins and core, see also [23]. Dimpling and wrinkling modes are characterized by a very short wavelength along the in-plane directions x_1, x_2; some model assessments in Section 7 will address this short wavelength response.

3. Classical theories: CLPT and FSDT

This section presents the fundamental equations of the classical plate theories formulated within the axiomatic, displacement-based approach outlined in the previous Section. *Classical theories* are the Classical Laminated Plate Theory (CLPT) and the First-order Shear Deformation Theory (FSDT), the difference being in the way transverse shear strain is accounted for. These theories rely on an ESL description and are essentially a straightforward application to composite plates of theories formulated for homogeneous plates. For an exhaustive presentation of CLPT and FSDT reference can be made to Reddy's book [24].

3.1. Classical Laminated Plate Theory

The CLPT is an application to composite plates of the classical thin plate theory originally developed for homogeneous plates. It can be axiomatically formulated based on the following *a priori* assumptions [3]:

1. Kinematic assumption: *fibers that are straight and perpendicular to the reference surface of the undeformed plate, remain straight and perpendicular to* Ω *during deformation* (Kirchhoff's assumption).
2. Static assumption: *the transverse normal stresses are negligibly small compared to the bending stresses.*

Kirchhoff's assumption means neglecting the transverse shear deformation of the plate:

$$\epsilon_4 = u_{3,_2} + u_{2,_3} = 0 \qquad \epsilon_5 = u_{3,_1} + u_{1,_3} = 0 \tag{20}$$

On the other hand, within a displacement-based approach, the static assumption requires to be recast in a kinematic relationship through the use

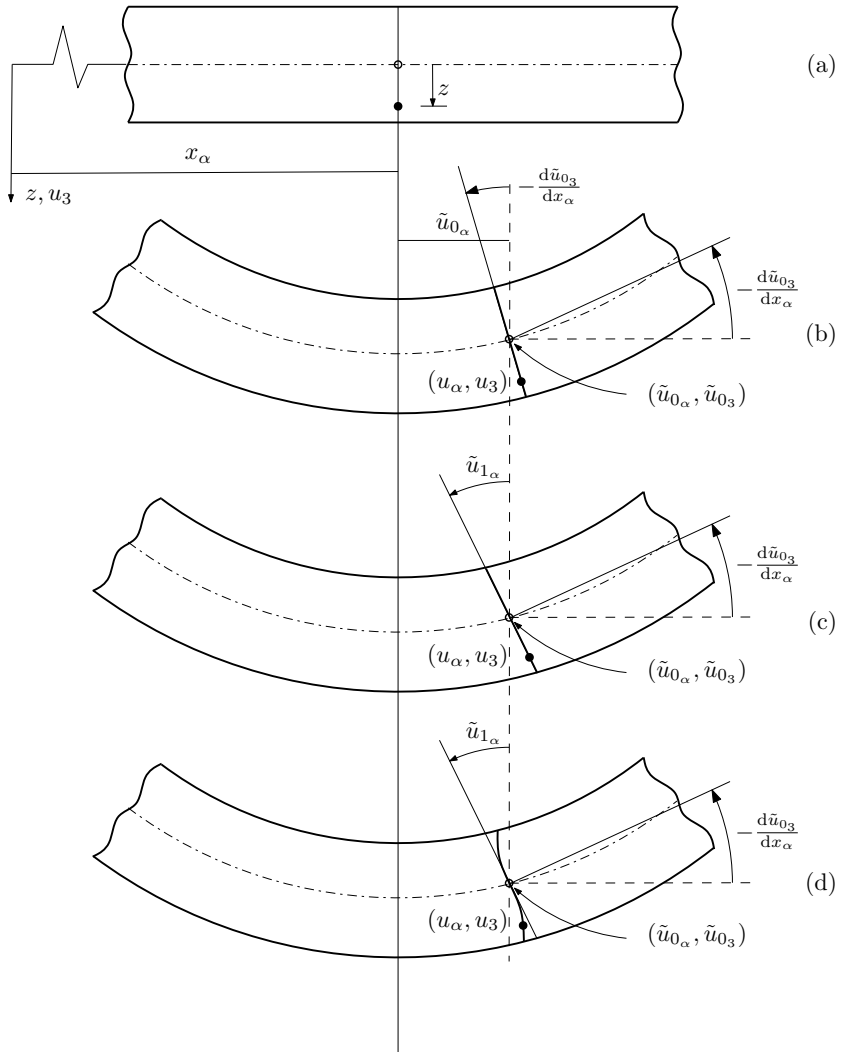

Figure 2: Transverse normal fiber in its undeformed configuration (a), and in the deformed configuration according to three different kinematics: (b) CLPT; (c) FSDT; (d) HSDT.

of the constitutive stress-strain relation. Imposing the condition $\sigma_3 = 0$ into Hooke's law Eq. (4) of the composite plate yields

$$\epsilon_3^{(p)} = -\frac{C_{13}^{(p)}}{C_{33}^{(p)}}\epsilon_1 - \frac{C_{23}^{(p)}}{C_{33}^{(p)}}\epsilon_2 - \frac{C_{36}^{(p)}}{C_{33}^{(p)}}\epsilon_6 \tag{21}$$

and the following *plane stress* constitutive relation:

$$\begin{bmatrix} \sigma_1^{(p)} \\ \sigma_2^{(p)} \\ \sigma_6^{(p)} \end{bmatrix} = \begin{bmatrix} Q_{11}^{(p)} & Q_{12}^{(p)} & Q_{16}^{(p)} \\ & Q_{22}^{(p)} & Q_{26}^{(p)} \\ \text{sym} & & Q_{66}^{(p)} \end{bmatrix} \begin{bmatrix} \epsilon_1 \\ \epsilon_2 \\ \epsilon_6 \end{bmatrix} \tag{22a}$$

where $Q_{pq}^{(p)}$ $(p, q \in \{1, 2, 6\})$ are the "reduced" stiffness coefficients of the ply (p) defined as

$$Q_{pq}^{(p)} = C_{pq}^{(p)} - \frac{C_{p3}^{(p)} C_{q3}^{(p)}}{C_{33}^{(p)}} \qquad \text{for } p, q \in \{1, 2, 6\} \tag{22b}$$

Note that, by virtue of the monoclinic symmetry of each ply, see Eq. (5), setting to zero the transverse shear strains corresponds to let the transverse shear stress be nil as well. The kinematic assumption expressed by Eq. (21) means that the transverse normal strain is independent from the out-of-plane deflection u_3, which can hence be assumed as independent from the $z-$coordinate, recall Eq. (1). With reference to the generic assumptions expressed by Eq. (6), one may thus set

$$N_3 = 0 \quad \text{with } F_{0_3}(z) = 1 \tag{23a}$$

Furthermore, the vanishing of the transverse shear strains postulated by Kirchhoff's assumption Eq. (20) means that the transverse fiber rigidly rotates about the x_1 and x_2 directions, and that this rotation is directly linked to the slope of the reference surface, see Fig. 2 (b). With reference to Eq. (6) these relations are satisfied by setting for the in-plane displacements u_α

$$N_\alpha = 1; \quad F_{0_\alpha}(z) = 1, \; F_{1_\alpha}(z) = z \quad \text{with } \alpha \in \{1, 2\} \tag{23b}$$

along with the normality condition of Kirchhoff's assumption

$$\tilde{u}_{1_\alpha} = -u_{3,\alpha} \tag{23c}$$

The displacement field of the CLPT has, hence, the following form:

$$u_\alpha(x_1, x_2, z; t) = \tilde{u}_{0_\alpha}(x_1, x_2; t) - z\,\frac{\partial \tilde{u}_{0_3}(x_1, x_2; t)}{\partial x_\alpha} \qquad (\alpha \in \{1, 2\}) \tag{24a}$$

$$u_3(x_1, x_2, z; t) = \tilde{u}_{0_3}(x_1, x_2; t) \tag{24b}$$

with three unknown functions defining the displacement vector of a generic point of the reference surface Ω: two functions $\tilde{u}_{0_\alpha}(x_1, x_2; t)$ define the membrane deformation and only one function $\tilde{u}_{0_3}(x_1, x_2; t)$ defines the bending deformation. In view of a FEM approximation, a drawback of the CLPT is its need for a C^1-continuous interpolation of the transverse displacement.

3.2. First-order Shear Deformation Theory

The *a priori* assumptions of FSDT read as follows:

1. Kinematic assumption: *fibers that are straight and perpendicular to the reference surface of the undeformed plate, remain straight but not necessarily perpendicular to* Ω *during deformation.*
2. Static assumption: *the transverse normal stresses are negligibly small compared to the bending stresses.*

The first assumption relaxes the normality condition of Kirchhoff's assumption; FSDT enhances CLPT upon including a shear deformation that is constant (i.e., first order) with respect to the thickness coordinate. The static assumption $\sigma_3 = 0$ is still retained. Therefore, the relation Eq. (21) still holds and the constitutive equation to be used is Eq. (22) complemented by the transverse shear terms

$$\begin{bmatrix} \sigma_4^{(p)} \\ \sigma_5^{(p)} \end{bmatrix} = \begin{bmatrix} Q_{44}^{(p)} & Q_{45}^{(p)} \\ \text{sym} & Q_{55}^{(p)} \end{bmatrix} \begin{bmatrix} \epsilon_4 \\ \epsilon_5 \end{bmatrix} \tag{25}$$

In order to instantiate the general displacement assumptions Eq. (6) for the FSDT case, it is first noticed that the plane stress assumption yields the same approximations given in Eq. (23a) for the out-of-plane displacement u_3. Furthermore, a transverse shear deformation that is constant across the plate thickness means that the normal fiber still remains rigid, which is expressed by Eq. (23b). However, the rotation about the x_α directions is no longer directly related to the slope of the reference surface, i.e., the unknown functions $\tilde{u}_{1_\alpha}(x_1, x_2; t)$ associated to the linear term F_{1_α} are now additional independent functions, see Fig. 2 (c). By denoting φ_α the positive rotations about the axis x_α, one has $\tilde{u}_{1_2} = \varphi_1$ and $\tilde{u}_{1_1} = -\varphi_2$. The displacement field of the FSDT has thus the following expression:

$$u_\alpha(x_1, x_2, z; t) = \tilde{u}_{0_\alpha}(x_1, x_2; t) + z\, \tilde{u}_{1_\alpha}(x_1, x_2; t) \qquad (\alpha \in \{1, 2\}) \tag{26a}$$

$$u_3(x_1, x_2, z; t) = \tilde{u}_{0_3}(x_1, x_2; t) \tag{26b}$$

The following expression is obtained for the transverse shear strains, that turn out to be independent of z:

$$\gamma_{\alpha 3}(x_1, x_2, z; t) = \tilde{u}_{1_\alpha}(x_1, x_2; t) + \frac{\partial \tilde{u}_{0_3}(x_1, x_2; t)}{\partial x_\alpha} = \gamma_{\alpha 3}^0(x_1, x_2; t) \tag{27}$$

The number of independent two-dimensional functions of FSDT is thus 5: the 2 functions $\tilde{u}_{0_\alpha}$ define the membrane and 3 functions $\tilde{u}_{1_\alpha}, \tilde{u}_{0_3}$ the bending deformation. An attractive feature of FSDT is that its FEM implementation requires only C^0 interpolations. However, a special treatment is needed for the evaluation of the transverse shear deformation for avoiding the shear locking pathology [25].

Numerical shear correction factors $k^s_{ij} < 1$ with $i, j \in \{4, 5\}$ should be introduced in the computation of the transverse shear force, in order reduce the transverse shear deformation energy that is overestimated by the first-order approximation, for it violates the shear stress-free conditions at the outer surfaces of the plate, viz. $\sigma_4 = \sigma_5 = 0$ at $\Gamma_\pm$. For homogeneous plates ($k^s_{45} = 0, k^s_{44} = k^s_{55} = k^s$) Reissner's static approach yields the value $k^s = 5/6$ for a bending problem [26], while Mindlin obtained the value $k^s = \pi^2/12$ by equating the approximate first antisymmetrical thickness-shear vibration frequency to the exact solution [27]. However, the proper choice of these numerical factors is actually problem-dependent [28–30].

4. Refined ESL theories

Due to their simplicity, the classical theories outlined in the preceding section are the most widespread but, at the same time, their accuracy is often limited. The following statement of Koiter can be taken as a valuable guideline for enhancing the model accuracy [31]: "A refinement of [...] first approximation theory is indeed meaningless, in general, unless the effects of transverse shear and normal stresses are taken into account at the same time." This section presents refined ESL theories according to the following classification: (1) theories that enhance the approximation of the transverse shear deformation of FSDT; (2) ESL models that meet the so-called C^0_z-Requirements [32], i.e., the piecewise continuous distribution of displacement and transverse stress fields along the thickness direction z of a composite stack, see Fig. 3; (3) theories including the transverse normal stress, thus aiming at a consistent extension of the models to high-order accuracy according to Koiter.

4.1. Higher-order Shear Deformation Theories

HSDT enhance the classical theories upon relaxing the kinematic assumption that straight fibers remain straight during deformation, which means that the normal fiber can *warp* during deformation. This is accomplished by postulating a non-linear (high-order) distribution of the in-plane displacement along the thickness direction of the whole composite plate, i.e., an ESL description is still retained. The warping function should allow an at least

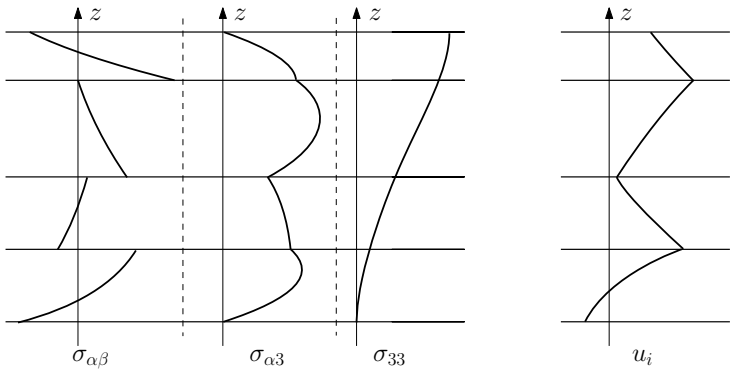

Figure 3: Typical distributions along the thickness satisfying the 3D elasticity equations: in-plane stresses $\sigma_{\alpha\beta}$ are C_z^{-1}, transverse shear stresses $\sigma_{\alpha 3}$ are C_z^0, transverse normal stress σ_{33} is C_z^1, and displacements u_i are C_z^0.

quadratic distribution of the transverse shear stress in order to fulfill the shear stress-free conditions at the plate's top and bottom surfaces. This way, shear correction factors are no longer required. The static assumption $\sigma_3 = 0$ of classical theories is still retained. A general representation of the assumed displacement field of an HSDT can be written as follows [33, 34]:

$$u_\alpha(x_1, x_2, z; t) = \tilde{u}_{0_\alpha}(x_1, x_2; t) - z\,\frac{\partial \tilde{u}_{0_3}(x_1, x_2; t)}{\partial x_\alpha} + f(z)\left(\tilde{u}_{1_\alpha}(x_1, x_2; t) + \frac{\partial \tilde{u}_{0_3}(x_1, x_2; t)}{\partial x_\alpha}\right) \tag{28a}$$

$$u_3(x_1, x_2, z; t) = \tilde{u}_{0_3}(x_1, x_2; t) \tag{28b}$$

where $\tilde{u}_{1_\alpha} + \tilde{u}_{0_{3,\alpha}} = \gamma^0_{\alpha 3}$ is the z-independent transverse shear deformation of FSDT, see Eq. (27). Fig. 2 (d) illustrates a typical example of this high-order kinematics with the warped normal fiber. Different theories can be instantiated depending on the expression of the *warping function* $f(z)$:

1. Classical theories are recovered as special cases by setting $f(z) = 0$ for CLPT and $f(z) = z$ for FSDT.
2. The so-called Sinus-theory [35] is a seminal example of the family of trigonometric HSDT and is implemented by setting

$$f(z) = \frac{h}{\pi}\sin\left(\frac{\pi z}{h}\right) \tag{29}$$

A mathematical justification for using the Sinus function is provided in [36].

3. The third-order theory [24, 37, 38] is formulated with

$$f(z) = z - \frac{4z^3}{3h^2} \tag{30}$$

The third-order theory is the most representative example of polynomial HSDT, in which the warping function is a polynomial development in z.

The third-order theory accommodates a parabolic distribution of transverse shear stress, whereas the Sinus theory implies a transverse shear stress that varies as a Cosine across the plate thickness. The kinematics Eq. (28) yields the following expression for the transverse shear strains:

$$\gamma_{\alpha 3}(x_1, x_2, z; t) = \frac{\mathrm{d}f(z)}{\mathrm{d}z}\,\gamma^0_{\alpha 3}(x_1, x_2; t) \tag{31}$$

$$\text{with} \quad \begin{cases} \frac{\mathrm{d}f(z)}{\mathrm{d}z} = \cos\left(\frac{\pi z}{h}\right) & \text{Sinus theory} \\ \frac{\mathrm{d}f(z)}{\mathrm{d}z} = 1 - 4\left(\frac{z}{h}\right)^2 & \text{third-order theory} \end{cases}$$

where $\gamma^0_{\alpha 3}$ is the transverse shear strain of FSDT defined in Eq. (27). Note that both theories automatically ensure zero transverse shear stresses at the top and bottom surfaces of the plate ($z = \pm h/2$). Furthermore, it should be remarked that the number of unknown functions in both theories is equal to 5, the same number of unknown functions of FSDT. However, these HSDT finite elements require – as CLPT-based elements – a C^1 approximation for the transverse deflection.

4.2. Zig-Zag theories

ZZT enhance the through-the-thickness response of composite structures upon formulating a kinematics that can represent the slope discontinuity of the in-plane displacements at interfaces between adjacent plies. In an important reference paper, Carrera summarizes the major developments of ZZT and identifies three independent paths for meeting the C^0_z-requirements [16]: Lekhnitskii Multilayered Theory (LMT), Ambartsumian Multilayered Theory (AMT) and Reissner Multilayered Theory (RMT). In this section the focus is set on AMT, the most widespread approach, and RMT that is the most amenable to further extensions due to its simplicity.

Ambartsumian Multilayered Theory. A piecewise continuous displacement field is constructed whose interlaminar continuity conditions are issued from the continuity conditions of the transverse shear stresses. So, *a priori* assumptions are postulated for the transverse stress field and converted to a

kinematic field through the constitutive law, which is thus exactly verified in this approach. The AMT extends FSDT upon replacing the kinematic assumption with the following

1. Static assumption: *The transverse shear stresses has a parabolic distribution along the thickness of each ply.*

As in the previously outlined theories, the first assumption calls for the use of the *plane stress* constitutive law. The second assumption introduces a number of parameters that depend on the number of plies, but these are explicitly determined through the continuity conditions of the transverse shear stresses and of the displacement field. The resulting kinematics, not reported here for the sake of brevity, has the same 5 unknown functions of FSDT and does explicitly depend on the material parameters of the plies constituting the composite plate. The dependence of the kinematics on the material parameters makes the extension of AMT to more complex material behaviors, such as those involving multifield couplings, quite a cumbersome task. The AMT approach is generally limited for postulating a zig-zag shape for the in-plane displacements only; its extension to a piecewise continuous out-of-plane displacement is not possible if the constitutive law is to be exactly verified, because the Poisson coupling between the transverse stretch and the in-plane deformations prevents the expression of a zig-zag kinematics.

Reissner Multilayered Theory. In RMT, independent assumptions are formulated for displacement and transverse stresses by referring to Reissner's Mixed Variational Theorem (RMVT) [14]. The seminal formulation is due to Murakami [39], who used the same static assumptions of AMT ($\sigma_{\alpha 3}$ parabolic in each ply) in conjunction with the following kinematics:

$$u_\alpha(x_1, x_2, z; t) = \tilde{u}_{0_\alpha}(x_1, x_2; t) + z\tilde{u}_{1_\alpha}(x_1, x_2; t) + M_{ZZ}(z)\tilde{u}_{ZZ\,\alpha}(x_1, x_2; t) \tag{32a}$$

$$u_3(x_1, x_2, z; t) = \tilde{u}_{0_3}(x_1, x_2; t) \tag{32b}$$

The in-plane displacement field u_α is thus approximated upon enhancing the classical FSDT kinematics with the so-called Murakami Zig-Zag Function (MZZF), which permits to introduce in a simple geometrical manner the slope discontinuity at plies' interfaces:

$$M_{ZZ}(z) = (-1)^p\,\zeta_p(z) \quad \text{with} \quad \zeta_p(z) = \frac{2}{z_p^t - z_p^b}\left(z - \frac{z_p^t + z_p^b}{2}\right) \tag{33}$$

where z_p^t and z_p^b denote the top and bottom $z-$coordinates of the p^{th} ply. Fig. 4 illustrates the kinematics Eq. (32a) resulting from the superposition

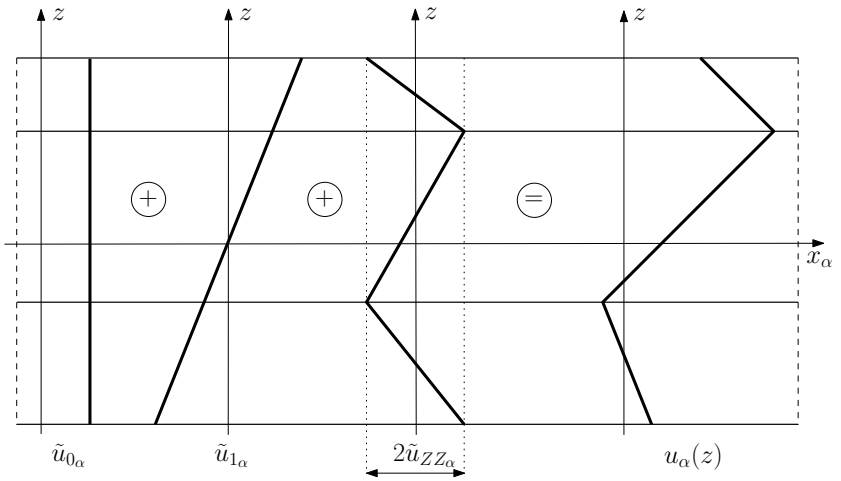

Figure 4: Kinematics resulting from the superposition of FSDT (membrane term $\tilde{u}_{0_\alpha}$ and bending term $\tilde{u}_{1_\alpha}$) and MZZF (amplitude $\tilde{u}_{ZZ_\alpha}$ of the Zig-Zag function).

of MZZF on an FSDT approximation. The integral of RMVT along the thickness direction is carried out explicitly, which provides the weak form of the equilibrium equations as well as the weak form of the constitutive relationship for the composite plate linking transverse shear stresses and displacement field. This "weak form of Hooke's law" (*i*) automatically incorporates the necessary shear correction factors for the underlying FSDT kinematics, and (*ii*) can be conveniently used to obtain a formulation involving only unknown functions related to displacement variables, see also [15]. The ZZT resulting from Eq. (32) has 7 unknown functions, i.e., the 5 functions of FSDT plus the 2 functions $\tilde{u}_{ZZ\,\alpha}$ that define the amplitude of MZZF. It is worth emphasizing that this approach can be extended in a straightforward manner to transverse normal strains and complex material behaviors because the constitutive relations are satisfied only in an integral, variationally consistent sense [40, 41].

Later developments suggested to formulate ZZT by directly superimposing MZZF to a simple ESL kinematics within a classical displacement-based approach [42]. In this "simple" approach no reference is made to the transverse stress field that, as a consequence, does not verify the interlaminar equilibrium nor the top and bottom conditions.

4.3. Theories including transverse normal stress

All previously discussed theories rely on the static assumption $\sigma_3 = 0$ and make use of the plane stress constitutive law Eq. (22); this leads to a model in which the through-thickness stretch is only a reactive deformation.

This section discusses those advanced theories that, following Koiter's recommendation, include the transverse normal stress and strain by using the full three-dimensional constitutive law Eq. (4).

It is first remarked that, in bending-dominated problems, the linear distribution of in-plane strains requires an at least linear transverse normal strain for consistently representing the Poisson effect, see Eq. (21). Therefore, an at least quadratic approximation for the transverse displacement is necessary, i.e., $N_3 \geq 2$ must be taken in Eq. (6) for avoiding the so-called thickness or Poisson locking [43]. This condition has been identified through asymptotic analyses as well [44, 45]. Choosing $N_\alpha = N_3 - 1$ for the in-plane displacement field ($\alpha \in \{1, 2\}$), allows a consistent representation of the Poisson coupling in Eq. (21). However, in bending-dominated problems it is often more important to enhance the transverse shear strain distribution, and the choice $N_\alpha = N_3 + 1$ would be preferred. A seminal example is given by the $\{N_\alpha, N_3\} = \{3, 2\}$ theory of [46]:

$$u_\alpha(x_1, x_2, z; t) = \sum_{s=0}^{3} z^s \, \tilde{u}_{s_\alpha}(x_1, x_2; t) \tag{34a}$$

$$u_3(x_1, x_2, z; t) = \sum_{s=0}^{2} z^s \, \tilde{u}_{s_3}(x_1, x_2; t) \tag{34b}$$

In closure to this section two Sinus-based high-order kinematics are mentioned, which include transverse normal stretch and Zig-Zag effect [47, 48]. These models will be included in the numerical assessment proposed in Section 7. In [47], the Zig-Zag effect has been included according to AMT and does not affect the transverse deflection; the importance of the out-of-plane deformation has been pointed out in conjunction with thermal stress problems. The model proposed in [48] introduces the Zig-Zag effect by means of MZZF; a slope discontinuity is thus included in the out-of-plane deflection, which has been shown to play a crucial role for a consistent refined modeling of the piezoelectric bimorph bending actuator.

5. Layer-Wise models

Displacement-based LW models subdivide the composite stack into N_l layers and introduce the approximated kinematics Eq. (6) for each layer $l = 1, 2, \ldots N_l$ separately:

$$u_i^{(l)}(x_1, x_2, z; t) = F_{s_i}(z) \tilde{u}_{s_i}^{(l)}(x_1, x_2; t) \qquad \text{with } s_i = 0, 1, 2, \ldots N_i^{(l)} \tag{35}$$

The resulting model for the whole composite stack is thus obtained as an assembly of LW approximations and the number of unknown functions depends on the number of layers the composite stack has been subdivided into. The assembly procedure assures the continuity of the displacement field at the layers' interfaces. A common choice is to let the layers be coincident with the physical plies constituting the composite, i.e., to set $N_l = N_p$. For a refined representation, each physical ply may be decomposed in several layers, i.e., $N_l > N_p$; alternatively, several physical plies can be grouped into one layer, which will be referred to as a *sublaminate*, and in this case one has $N_l < N_p$.

Reddy's model is by far the most representative LW model [24, 49, 50]; it employs Lagrange polynomials for interpolating the displacement field inside each layer. A linear LW assumption is obtained from the general expression Eq. (35) as follows

$$\forall i \in \{1,2,3\}: \quad N_i = 1; \quad F_{0_i}(z) = \frac{1-\zeta_l(z)}{2}; \quad F_{1_i}(z) = \frac{1+\zeta_l(z)}{2} \tag{36}$$

where $\zeta_l(z)$ is the layer-specific dimensionless coordinate defined as in Eq. (33). There are two reasons for preferring a Lagrange interpolation over Taylor's expansion: (i) it allows a direct access to the top and bottom displacements and, hence, a straightforward assembly procedure; (ii) it enforces a mere C^0 continuity at layers' interfaces, which complies with the characteristic zig-zag effect of composite stacks. Similar to FEM, refined approximations inside each layer can be introduced by subdividing it into several layers ($h-$refinement) or upon enhancing the interpolation order ($p-$refinement).

Due to their refined description, LW models that retain the full three-dimensional constitutive behavior permit to obtain a quasi-3D response of the composite plate, see, e.g., [51]. One of the advantages of LW models over the standard 3D modeling relies in the less cumbersome two-dimensional data structure and in the independent approximations that can be used for the reference surface Ω and the thickness. However, their computational cost may be high if the composite is composed of a large number of layers.

6. Unified Formulation

As early recognized by Reddy [49], all models discussed so far can be formally represented by the general expression given in Eq. (35). Note that ESL models can be obtained from the LW expression Eq. (35) by setting $N_l = 1$. A computer program can thus be written in which the parameters that define the model are let free to be chosen by the user at "run time".

This is the underlying idea of *Unified Formulations* first proposed by Carrera [52] and that have attracted much interest in view of its great flexibility.

Carrera's Unified Formulation (CUF) proposes ESL and LW structural models formulated within the PVD or within RMVT. The displacement field can be described either as ESL or LW, transverse stresses are always taken LW. ESL models employ Taylor's expansion whereas LW models employ approximating functions defined by Legendre's polynomials; Zig-Zag models are formulated by means of MZZF. Furthermore, the same expansion order is used for all variables involved in the dimensional reduction (displacements and, for RMVT-based models, transverse stresses), and individual terms of the expansion may be suppressed through opportune penalizations [53].

Demasi extended CUF to explicitly formulate models in which the order of expansion can be chosen independently for each displacement/transverse stress component [54, 55]. In his Generalized Unified Formulation (GUF), Demasi further provides the possibility of describing some displacement components in an ESL manner and others in an LW manner (partially LW models) [56].

A further extension of GUF has been recently proposed, which introduces the possibility of subdividing the composite stack into sublaminates, which means that the ESL/LW description and the expansion order of each variable can be independently chosen in each sublaminate [57]. The possibility of an ESL description of the transverse stresses has been accounted for as well. This so-called Sublaminate-GUF (S-GUF) appears as particularly meaningful for the modeling of sandwich structures, for which it appears as a natural choice to formulate "three-layers models": different assumptions are made for the behavior of the thin, stiff skins and the thick, compliant core layers [58].

7. Assessment on some benchmark problems

In this last section, several of the previously discussed theories are evaluated and compared on some benchmark problems involving both laminated and sandwich plates. The accuracy is assessed in terms of long wavelength response that includes global quantities, such as fundamental natural frequencies and global buckling loads, as well as local quantities, such as point displacement and stress; the short wavelength response of sandwich wrinkling is also considered. In order to permit a direct comparison with elasticity solutions, attention is restricted to rectangular plates with simple-support conditions and material orthotropy.

Section 7.1 deals with bending and vibration problems with reference to classical benchmark problems introduced by Pagano [59]. The influence of

the geometric span-to-thickness ratio a/h on the accuracy of the various ESL and LW plate models is evaluated.

The elastic instability of sandwich plates subjected to uniaxial compression is investigated in Section 7.2 in a plane strain setting. The accuracy of the buckling load and mode predicted by several models is assessed with respect to the geometric thickness ratio h_f/h_c and the stiffness ratio E_f/E_c between the face and core materials.

Due to the large variety of refined ESL models proposed in literature, it is worthwhile summarizing those employed in the following assessment. Tab. 1 lists the considered models introducing a unique denomination and specifying the number of unknown functions (parameters). The proposed denomination is constituted by an acronym that contains the key properties of the model according to the presentation in Section 4:

- A "T" followed by two integers for a Taylor-based polynomial expansion of the kinematics; the first integer indicates the order of the in-plane displacement expansion, the second integer that of the transverse displacement. The second integer may be zero if the plane stress assumption is retained, or two if the full 3D constitutive law is used.

- An "S" followed by one integer if the Sinus function is used for the transverse shear; the integer specifies the expansion order of the transverse displacement (as before, either 0 or 2).

- A "Z" is added if the Zig-Zag effect is retained in the in-plane displacements; a "ZZ" is used if the Zig-Zag is retained for the transverse deflection as well.

- A "C" is added if the transverse shear stress is continuous at interfaces between plies.

7.1. Bending and vibration of composite plates

Several classical and refined ESL models are assessed with respect to a long wavelength response of laminated and sandwich plates. The local response is considered by referring to the classic Pagano problems of simply-supported rectangular plates bent by a pressure load. The global response is addressed by referring to the fundamental flexural vibration frequencies. All presented results are converged FEM solutions computed with robust finite elements free of numerical pathologies. These solutions are compared against exact elasticity solutions obtained according to the methods proposed by Pagano [59] for the bending problem and by Loredo [62] for the free-vibration problem.

Acronym	ZZT approach	Const. law	Parameters	Ref
Kinematics based on Sinus function				
S0	–	2D	5	[35]
S0ZC	AMT	2D	5	[60]
S2	–	3D	9	[48]
S2ZC	AMT	3D	11	[47]
S2Z	MZZF	3D	11	[48]
S2ZZ	MZZF	3D	12	[48]
Kinematics based on Taylor expansion				
CLPT	–	2D	3	[24]
FSDT	–	2D	5	[24]
T10ZC	RMT	2D	7	[61]
T30	–	2D	9	[37]†
T32	–	3D	11	[46]
T32ZZ	MZZF	3D	14	[56]

† *kinematics of Eq.(1) in [37]:* $\gamma_{\alpha 3}(z = \pm\frac{h}{2}) = 0$ *is not enforced.*

Table 1: Acronyms and main features of the ESL models used in the assessment.

The proposed assessment aims at comparing the accuracy of classical CLPT and FSDT models, refined HSDT, and other advanced theories with particular emphasis on the effect of the following assumptions: inclusion of Zig-Zag effect on the in-plane displacements only or on all displacement components; inclusion of Zig-Zag effect with or without accounting for the interlaminar continuity of the transverse shear stresses; use of the three-dimensional constitutive law with the inclusion of a through-thickness stretch through a quadratic expansion along z for the transverse displacement.

Laminated plates. The assessment is here proposed for symmetric and non-symmetric laminated plates with different length-to-thickness ratios, according to the following configurations:

geometry a rectangular plate of in-plane dimensions $a \times b$ with $b = 3a$ made out of two plies of equal thickness $h/2$;

a square plate $a \times a$ made out of three plies of equal thickness $h/3$;

in either case, the length-to-thickness ratios are $S = \dfrac{a}{h} = 4, 10, 100$

boundary conditions simply supported on all sides; for the bending problem, a bi-sinusoidal transverse distributed load is applied at the top

surface $p_3(x_1, x_2, z = \dfrac{h}{2}) = p_0 \ \sin\dfrac{\pi x_1}{a} \ \sin\dfrac{\pi x_2}{b}$

materials cross-ply laminates with stacking sequence (from bottom) $(0°, 90°)$ and $(0°, 90°, 0°)$; engineering moduli of each transversely isotropic ply: $E_L = 25\ GPa, E_T = 1\ GPa, \nu_{LT} = \nu_{TT} = 0.25, G_{LT} = 0.2\ GPa, G_{TT} = 0.5\ GPa$; mass density $\rho = 1500\ kg/m^3$

results displacements and stresses are made non-dimensional according to

$$\begin{aligned}
\bar{U}_\alpha &= U_\alpha \ \frac{E_T}{p_0 \ h \ S^3} \quad \text{for} \ \begin{cases} U_1(0, a/2, z) \\ U_2(a/2, 0, z) \end{cases} \\
\bar{U}_3 &= U_3(a/2, a/2, z) \ \frac{100 \ E_T}{p_0 \ h \ S^4} \\
\bar{\sigma}_{\alpha\beta} &= \sigma_{\alpha\beta} \ \frac{1}{p_0 \ S^2} \quad \text{for} \ \begin{cases} \sigma_{11}(a/2, b/2, z), \sigma_{22}(a/2, b/2, z) \\ \sigma_{12}(0, 0, z) \end{cases} \\
\bar{\sigma}_{\alpha 3} &= \sigma_{\alpha 3} \ \frac{1}{p_0 \ S} \quad \text{for} \ \begin{cases} \sigma_{13}(0, b/2, z) \\ \sigma_{23}(a/2, 0, z) \end{cases}
\end{aligned} \tag{37a}$$

The eigenfrequency is made non-dimensional according to

$$\bar{\omega} = \omega \ \frac{a^2}{h} \ \sqrt{\frac{E_T}{\rho}} \tag{37b}$$

reference values are the three-dimensional exact elasticity results.

Tab. 2 presents the first natural frequencies (global response) for both stacking sequences; Tab. 3 and Tab. 4 give displacements and stresses (local response) for the non-symmetric 2-ply and the symmetric 3-ply laminate, respectively.

In Tab. 2, all models give accurate results for the thin plate case ($S = 100$). For $S = 10$, the error with respect to the reference solution for (2, 3) plies is $(0.9, 9.3)\%$ for FSDT and $(6.2, 31.8)\%$ for CLPT. Note that the stacking sequence has an influence on the response of the models. It can be stated that the classical models are not robust and must be used carefully. For these moderately thick plates, refined models give error less then 3%. For the thick case $S = 4$, the maximum error of the refined models increases up to 4.5%. The most accurate model is S2ZC. The influence of the expansion in the transverse direction can be appreciated by comparing S0ZC and S2ZC. The Zig-Zag effect associated to interlaminar discontinuous transverse shear deformations could be assessed by looking at S2 and S2Z. Note that S2Z

	2 plies $(0°, 90°)$			3 plies $(0°, 90°, 0°)$		
S	4	10	100	4	10	100
Ref	4.6573	5.9552	6.3675	6.9161	11.457	15.165
S2ZC	4.6640	5.9561	6.3677	6.9205	11.458	15.165
S2ZZ	4.7407	5.9840	6.3681	6.9428	11.461	15.166
S2Z	4.7410	5.9841	6.3682	6.9428	11.461	15.166
S2	4.7874	5.9973	6.3683	7.1021	11.723	15.173
S0ZC	4.8948	6.0353	6.3684	6.9938	11.457	15.165
S0	4.8418	6.0085	6.3681	7.0908	11.745	15.173
FSDT	4.8208	6.0099	6.3682	7.8756	12.527	15.191
CLPT	6.0865	6.3242	6.3716	14.500	15.104	15.226

Table 2: First natural frequency of cross-ply laminates.

and S2ZZ provide practically the same results for both laminates: the Zig-Zag term in the transverse direction can introduce a discontinuity of the transverse normal deformation, which could be useful if the ratios $C_{\alpha 3}/C_{33}$ change between adjacent plies, see Eq. (21). This is not the case here, the effect of this term is best highlighted in multi-field problems [48].

The local response is presented in Tab. 3 and Tab. 4. For $S = 100$, the displacements and in-plane stresses are predicted by all models with similar accuracy, but transverse shear stress values are very different. Recall that CLPT neglects these components, while FSDT gives constant values per layer (no shear correction factors are used throughout this assessment). Therefore, these models must be used with caution and only for thin plates.

For moderately thick and thick plates, and regarding advanced theories, the inclusion of the Zig-Zag effect always improves the displacement and stress results. This can be seen in Tab. 3 and Tab. 4 by comparing the models S0 and S2 on the one side, with S0ZC and S2ZC or S2ZZ on the other side. The challenge for these test configurations is related to the obtention of accurate results for the transverse shear stresses; best results are again recovered by the S2ZC model, followed by the S2Z (or S2ZZ).

The discrete values at specific locations are proposed to evaluate the accuracy of the models. It is, however, very useful to check the whole distribution across the composite stack also: Fig. 5 reports in-plane and transverse displacements and stresses for the thick, 3-ply symmetric plate. Despite the difference between S2ZC and S2ZZ was not really obvious in the tables, the continuity conditions verified only by the former model are clearly visible on the distribution of the transverse shear stress in Fig. 5 (right bottom). The distribution of the in-plane displacement $\bar{U}_1$ in Fig. 5 (left top) illustrates the

z	$\bar{U}_1$ (h/2)	$\bar{U}_2$ (-h/2)	$\bar{U}_3$ (0)	$\bar{\sigma}_{11}$ (-h/2)	$\bar{\sigma}_{22}$ (h/2)	$\bar{\sigma}_{12}$ (h/2)	$\bar{\sigma}_{13}$ (max)	$\bar{\sigma}_{23}$ (max)
S=4								
Ref	-0.0655	0.0271	4.3931	-1.7428	0.3306	-0.0498	0.6401	0.0762
S2ZC	-0.0656	0.0271	4.3820	-1.7856	0.3364	-0.0499	0.6492	0.0776
S2ZZ	-0.0619	0.0260	4.2388	-1.7161	0.3272	-0.0474	0.6094	0.0805
S2Z	-0.0619	0.0260	4.2420	-1.7161	0.3279	-0.0474	0.6099	0.0807
S2	-0.0543	0.0265	4.1733	-1.7803	0.3151	-0.0431	0.5543	0.0892
S0ZC	-0.0506	0.0238	3.9500	-1.9625	0.2966	-0.0418	0.4034	0.0648
S0	-0.0569	0.0258	4.1328	-1.9751	0.3093	-0.0456	0.6018	0.0931
FSDT	-0.0557	0.0271	4.4873	-1.6129	0.3035	-0.0447	0.4326	0.0665
S=10								
Ref	-0.0583	0.0211	2.7760	-1.6569	0.2277	-0.0412	0.6903	0.0600
S2ZC	-0.0583	0.0211	2.7754	-1.6624	0.2286	-0.0412	0.6921	0.0612
S2ZZ	-0.0576	0.0208	2.7492	-1.6585	0.2272	-0.0408	0.6272	0.0811
S2Z	-0.0576	0.0208	2.7494	-1.6588	0.2277	-0.0408	0.6275	0.0687
S2	-0.0562	0.0208	2.7378	-1.6721	0.2256	-0.0401	0.5688	0.0759
S0ZC	-0.0556	0.0204	2.7092	-1.6940	0.2226	-0.0398	0.4190	0.0579
S0	-0.0566	0.0208	2.7367	-1.6954	0.2250	-0.0404	0.6190	0.0787
FSDT	-0.0564	0.0210	2.7889	-1.6357	0.2250	-0.0403	0.4370	0.0532
S=100								
Ref	-0.0566	0.0196	2.4659	-1.6413	0.2067	-0.0393	0.7020	0.0562
S2ZC	-0.0566	0.0196	2.4657	-1.6421	0.2065	-0.0393	0.7022	0.0574
S2ZZ	-0.0566	0.0196	2.4656	-1.6470	0.2068	-0.0395	0.6328	0.0667
S2Z	-0.0566	0.0196	2.4655	-1.6473	0.2072	-0.0395	0.6330	0.0667
S2	-0.0566	0.0196	2.4653	-1.6474	0.2072	-0.0395	0.5734	0.0736
S0ZC	-0.0566	0.0196	2.4653	-1.6416	0.2067	-0.0393	0.4222	0.0562
S0	-0.0566	0.0196	2.4656	-1.6417	0.2067	-0.0393	0.6226	0.0753
FSDT	-0.0566	0.0196	2.4661	-1.6411	0.2067	-0.0393	0.4380	0.0501
CLPT	-0.0566	0.0196	2.4628	-1.6411	0.2065	-0.0393	-	-

Table 3: Bending of the rectangular $(0°, 90°)$ laminate under bi-sinusoidal load.

model z	$\bar{U}_1$ (h/2)	$\bar{U}_2$ (-h/2)	$\bar{U}_3$ (0)	$\bar{\sigma}_{11}$ (h/2)	$-\bar{\sigma}_{22}$ (-h/6)	$\bar{\sigma}_{12}$ (h/2)	$\bar{\sigma}_{13}$ (0)	$\bar{\sigma}_{23}$ (0)
S=4								
Ref	0.0094	0.0228	2.0059	0.8008	0.5563	0.0505	0.2559	0.2172
S2ZC	0.0097	0.0228	2.0080	0.8086	0.5583	0.0511	0.2556	0.2190
S2ZZ	0.0096	0.0229	1.9950	0.7762	0.5520	0.0494	0.2572	0.1858
S2Z	0.0096	0.0229	1.9950	0.7761	0.5518	0.0493	0.2572	0.1858
S2	0.0095	0.0221	1.9051	0.7705	0.5084	0.0483	0.2118	0.1857
S0ZC	0.0107	0.0218	1.9622	0.8560	0.5838	0.0510	0.2774	0.1494
S0	0.0094	0.0229	1.9345	0.7554	0.5033	0.0507	0.2113	0.1877
FSDT	0.0054	0.0181	1.7758	0.4370	0.4774	0.0369	0.1201	0.1301
S=10								
Ref	0.0074	0.0111	0.7530	0.5906	0.2882	0.0290	0.3573	0.1228
S2ZC	0.0074	0.0111	0.7531	0.5915	0.2880	0.0288	0.3573	0.1232
S2ZZ	0.0074	0.0111	0.7526	0.5944	0.2890	0.0287	0.3622	0.1039
S2Z	0.0074	0.0110	0.7526	0.5944	0.2852	0.0289	0.3622	0.1039
S2	0.0073	0.0106	0.7192	0.5885	0.2746	0.0279	0.2745	0.1052
S0ZC	0.0075	0.0110	0.7533	0.5975	0.2908	0.0279	0.3744	0.0859
S0	0.0072	0.0106	0.7180	0.5727	0.2708	0.0279	0.2583	0.1059
FSDT	0.0064	0.0096	0.6693	0.5134	0.2536	0.0252	0.1363	0.0762
S=100								
Ref	0.0068	0.0068	0.4347	0.5393	0.1808	0.0214	0.3947	0.0828
S2ZC	0.0068	0.0068	0.4347	0.5393	0.1808	0.0214	0.3947	0.0831
S2ZZ	0.0068	0.0068	0.4347	0.5410	0.1814	0.0214	0.3979	0.0715
S2Z	0.0068	0.0068	0.4347	0.5410	0.1814	0.0214	0.3979	0.0715
S2	0.0068	0.0068	0.4343	0.5409	0.1812	0.0214	0.2987	0.0754
S0ZC	0.0068	0.0068	0.4347	0.5393	0.1808	0.0214	0.4081	0.0600
S0	0.0068	0.0068	0.4343	0.5390	0.1806	0.0214	0.2738	0.0764
FSDT	0.0068	0.0068	0.4337	0.5384	0.1804	0.0213	0.1416	0.0586
CLPT	0.0068	0.0068	0.4313	0.5387	0.1796	0.0213	-	-

Table 4: Bending of the square, symmetric $(0°, 90°, 0°)$ laminate under bi-sinusoidal load.

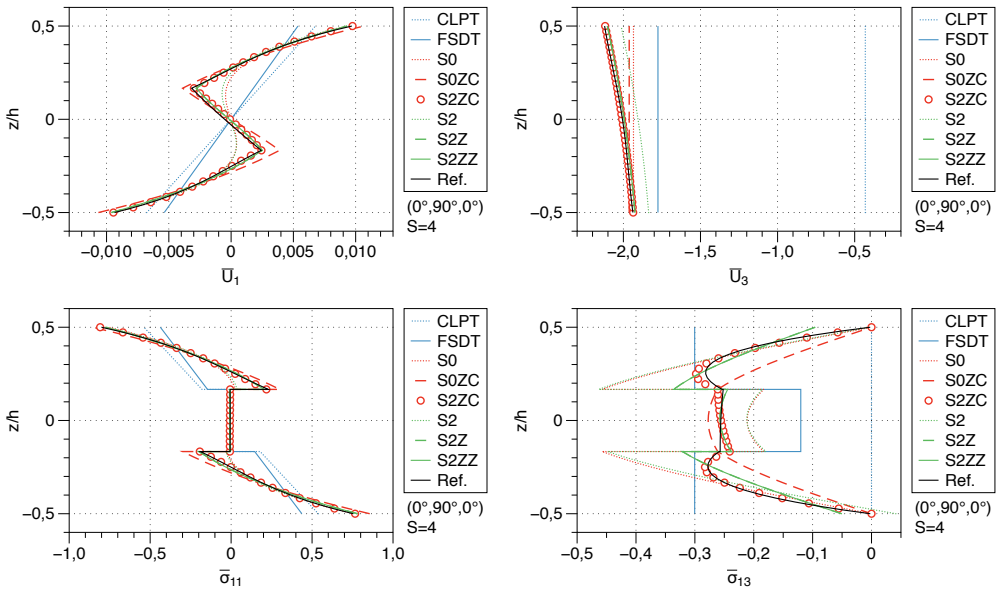

Figure 5: Local response for the thick ($S = 4$), square symmetric laminate $(0°, 90°, 0°)$ in bending: distributions along z of the non-dimensional in-plane and transverse displacement (top) and in-plane and transverse shear stress (bottom).

Zig-Zag effect; straight lines are associated with CLPT and FSDT, curved ones to S0 and S2, while all the other models integrating Zig-Zag distributions are close to the reference black line. Finally, the transverse displacement $\bar{U}_3$ across the thickness is presented in Fig. 5 (right top): this distribution is non linear, which illustrates the presence of a through-thickness stretch. Models of the S2-family can capture this effect, contrary to those based on the plane stress assumption (CLPT, FSDT, S0), which yield vertical straight lines. It is worth emphasizing that for this last distribution, the error for CLPT is 78.5% and that for FSDT is 11.5%.

Bending and vibration of a sandwich plate. Global and local response are next addressed for simply-supported sandwich square plates. The same pattern is followed as for the previously studied laminates: relevant quantities are the fundamental flexural vibration frequencies (global response) as well as the displacement and stress distributions (local response) under the action of a pressure load on the top surface; all presented results are converged FEM solutions, which are compared against exact elasticity solutions obtained according to [59] and [62] for the bending and the free-vibration problems, respectively.

Sandwich structures show quite a different behavior in comparison to laminates: the faces carry the primary bending stresses, the core assures the load transfer between the faces through transverse shear stresses [63]. Therefore, a Layer-Wise description is often considered as a necessary condition for recovering accurate results, especially for local responses and depending on the material (Young's modulus) and geometric (thickness) mismatch between faces and core. These parameters will be studied in Section 7.2 in conjunction with local and global buckling of sandwich structures. In the present analysis, the face-to-core Young's modulus ratio is fixed to 625 and the face-to-core thickness ratio to 0.125. The detail of the considered sandwich plate configuration is as follows [59]:

geometry sandwich square plate $a \times a$ and length-to-thickness ratios $S = \dfrac{a}{h} = 4, 10, 100$ with core thickness $h_c = 0.8\ h$ and face $h_f = 0.1\ h$

boundary conditions simply supported on all sides; for the bending problem, a bi-sinusoidal transverse distributed load is applied at the top surface $p_3(x_1, x_2, z = \dfrac{h}{2}) = p_0\ \sin\dfrac{\pi x_1}{a}\ \sin\dfrac{\pi x_2}{b}$

materials face properties $E_L = 25\ GPa, E_T = 1\ GPa, \nu_{LT} = \nu_{TT} = 0.25, G_{LT} = 0.5\ GPa, G_{TT} = 0.2\ GPa, \rho = 1500\ kg/m^3$

core properties $E_\alpha = 0.04\ GPa, E_3 = 0.5\ GPa, \nu_{12} = 0.25, \nu_{\alpha 3} = 0.02, G_{\alpha 3} = 0.06\ GPa, G_{12} = 0.016\ GPa, \rho_c = 100\ kg/m^3$

results displacements and stresses are made non-dimensional as in Eq. (37a); the natural frequency is made non-dimensional with the core properties according to

$$\bar{\omega} = \omega\ \frac{a^2}{h}\ \sqrt{\frac{E_2}{\rho_c}} \tag{38}$$

reference values are three-dimensional exact elasticity results.

Tab. 5 presents the first natural frequencies (global response) for different span-to-thickness ratios. For the thin plate case ($S = 100$), all models give accurate results. For $S = 10$, the error with respect to the reference solution is 23% and 57% for FSDT and CLPT, respectively. S0 and S2 models present both an error of 3%, while all models including the Zig-Zag effect are very accurate with an error less than 0.5%. The same comments are valid for the thick case $S = 4$. The following conclusions can be drawn: (i) the Zig-Zag effect is necessary for obtaining accurate results; (ii) the influence of the expansion in the transverse direction is less important than for laminates, as results given by S0 and S2 models are of the same order.

S	4	10	100
Ref	9.0871	17.150	27.147
S2ZC	9.1251	17.187	27.192
S2ZZ	9.1316	17.194	27.192
S2Z	9.1316	17.194	27.192
S2	9.4546	17.698	27.214
S0ZC	9.1108	17.168	27.148
S0	9.4292	17.694	27.171
FSDT	12.233	21.096	27.275
CLPT	18.831	26.918	27.366

Table 5: First natural frequency of the sandwich plate.

Displacement and stress values at relevant points are reported in Tab. 6 (local response). For $S = 100$, the displacements and maximum bending stresses in the faces are predicted by all models with similar accuracy. The transverse shear stress values, taken in the core, are strongly underestimated by FSDT, which provides only one third of the reference values. Again, CLPT and FSDT should thus be used with caution and only for displacements and in-plane stresses of thin sandwich plates. Comparing the models (S0, S2) with (S0ZC, S2ZC or S2ZZ), Tab. 6 highlights the importance of including the Zig-Zag effect in advanced theories for moderately thick and thick sandwiches. The local response also confirms that the inclusion of the transverse stretch plays a secondary role with respect to the transverse shear deformation.

z	$\bar{U}_1$ (-h/2)	$\bar{U}_2$ (-h/2)	$\bar{U}_3$ (0)	$\bar{\sigma}_{11}$ (h/2)	$-\bar{\sigma}_{22}$ (-h/2)	$\bar{\sigma}_{12}$ (-h/2)	$\bar{\sigma}_{13}$ (0)	$\bar{\sigma}_{23}$ (0)
S=4								
Ref	0.0184	0.0758	7.5962	1.5558	0.2533	0.1480	0.2387	0.1072
S2ZC	0.0183	0.0760	7.5883	1.5532	0.2608	0.1481	0.2377	0.1079
S2ZZ	0.0186	0.0827	7.5480	1.5204	0.2596	0.1596	0.2449	0.1089
S2Z	0.0184	0.0759	7.5748	1.5277	0.2699	0.1484	0.2471	0.1124
S2	0.0182	0.0838	7.0220	1.3957	0.1593	0.1602	0.2883	0.1192
S0ZC	0.0190	0.0756	7.6098	1.5589	0.2530	0.1486	0.2573	0.1198
S0	0.0175	0.0713	7.0928	1.4359	0.2382	0.1395	0.2832	0.1211
FSDT	0.0109	0.0469	4.7666	0.8918	0.1562	0.0907	0.1024	0.0448
S=10								
Ref	0.0143	0.0313	2.2004	1.1531	0.1099	0.0717	0.2998	0.0527
S2ZC	0.0142	0.0313	2.1946	1.1523	0.1131	0.0715	0.2991	0.0532
S2ZZ	0.0143	0.0323	2.1973	1.1568	0.1192	0.0735	0.3167	0.0553
S2Z	0.0143	0.0313	2.1922	1.1549	0.1147	0.0716	0.3167	0.0566
S2	0.0143	0.0314	2.0731	1.1388	0.0950	0.0718	0.3603	0.0592
S0ZC	0.0144	0.0311	2.1977	1.1555	0.1091	0.0713	0.3225	0.0589
S0	0.0141	0.0293	2.0681	1.1337	0.1034	0.0682	0.3465	0.0598
FSDT	0.0131	0.0221	1.5604	1.0457	0.0798	0.0552	0.1145	0.0245
S=100								
Ref	0.0138	0.0140	0.8924	1.0975	0.0550	0.0437	0.3240	0.0297
S2ZC	0.0138	0.0140	0.8895	1.0964	0.0568	0.0435	0.3236	0.0301
S2ZZ	0.0138	0.0140	0.8926	1.1027	0.0561	0.0438	0.3448	0.0316
S2Z	0.0138	0.0140	0.8895	1.1001	0.0570	0.0437	0.3445	0.0323
S2	0.0138	0.0140	0.8912	1.1024	0.0560	0.0438	0.3888	0.0350
S0ZC	0.0138	0.0140	0.8923	1.0975	0.0549	0.0437	0.3483	0.0335
S0	0.0138	0.0140	0.8908	1.0973	0.0549	0.0436	0.3705	0.0355
FSDT	0.0138	0.0139	0.8852	1.0964	0.0546	0.0435	0.1185	0.0178
CLPT	0.0138	0.0138	0.8782	1.0970	0.0543	0.0433	-	-

Table 6: Bending of a sandwich square plate under bi-sinusoidal load.

7.2. Buckling of sandwich struts

Buckling of sandwich struts is investigated in a two-dimensional plane strain setting (cylindrical bending) in the $(x_1\, z)-$plane. The initial stress is defined in each ply by a uniaxial compression produced by a uniform end shortening $\epsilon^0 < 0$ of the sandwich section:

$$N^0 = \int_{h_p} \sigma_p^0 \, \mathrm{d}z = \int_{h_p} C_{11}^{(p)} \epsilon^0 \, \mathrm{d}z \tag{39}$$

The full Green-Lagrange nonlinear strains of Eq. (17) are used for defining the geometric stiffness matrix. An exact solution along x_1 is found by referring to Navier's solution method.

The influence of the span-to-thickness ratio a/h on both global and local response has been investigated previously, this section thus focuses on the role of the specific ratios characterizing a sandwich plate, namely the thickness ratio h_f/h_c and the modulus ratio E_f/E_c between the face material and the core. Buckling is considered at a long wavelength (global buckling) as well as at a short wavelength (wrinkling), see Fig. 6. All models assessed in this section are obtained by the S-GUF software implemented by the authors and include ESL and LW models: Taylor-based ESL with and without Zig-Zag effect are considered following the notation introduced in Tab. 1; three-layers models are constructed as LW assemblies of individual ESL models. The denomination of three-layers models specifies the ESL model used for the faces and that used for the core, separated by a slash. It should be noted that, within S-GUF, the CLPT is obtained from FSDT upon penalizing the transverse shear strain energy, which means that the same number of parameters (5) is actually used in both theories. The three-layers models considered in the assessment are listed in Tab. 7 along with their total number of parameters.

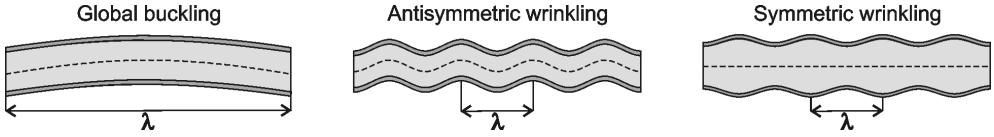

Figure 6: Global buckling and wrinkling modes of a sandwich strut.

Global buckling. The benchmark for the global buckling of the sandwich strut is defined as follows:

geometry strut of length a and thickness $h = 30\,mm$ with $a/h = 30$; face thickness defined by $h_f/h = 0.02, 0.04, 0.06, 0.08, 0.10, 0.12, 0.16, 0.20$.

Acronym (face/core)	Parameters
CLPT / FSDT	9
CLPT / T30	13
CLPT / T32	15
FSDT / T32	15

Table 7: Acronyms of the theee-layers models used for the sandwich buckling problems.

boundary conditions simple support at $x_1 = 0, a$.

materials orthotropic Graphite-Epoxy (Gr-Ep) faces: $E_{f1} = 181\,GPa, E_{f2} = E_{f3} = 10.3\,GPa, G_{f23} = 5.96\,GPa, G_{f13} = G_{f12} = 7.17\,GPa, \nu_{f23} = 0.400, \nu_{f13} = \nu_{f12} = 0.277$.

Orthotropic honeycomb core: $E_{c1} = E_{c2} = 32\,MPa, E_{c3} = 300\,MPa, G_{c23} = G_{c13} = 48\,MPa, G_{c12} = 13\,MPa, \nu_{c23} = \nu_{c13} = \nu_{c12} = 0.25$.

Isotropic PVC foam core: $\nu_c = 0.3$, E_c defined from the face-to-core stiffness ratio $E_{f1}/E_c = 200, 800, 1600, 2400, 3200, 4000$.

results the lowest critical load obtained for a mode characterized by one half-wave along x_1 ($m = 1$, global buckling) is made non-dimensional by normalizing it with the Euler load P_E of a beam:

$$P = \frac{N_{cr}}{P_E} \text{ with } P_E = \frac{\pi^2}{a^2}\left[E_{f1}h_f\left(\frac{h_f^2}{6} + \frac{(h_f + h_c)^2}{2}\right) + E_{c1}\frac{h_c^3}{12}\right] \quad (40)$$

reference values are elasticity solutions provided in [64]

The results in Tab. 8 refer to the Gr-Ep/honeycomb sandwich with variable face-to-core thickness ratio h_f/h. An excellent agreement with the reference solution of [64] is observed for all models that explicitly account for the representation of the face-core interface, either through a LW description or by means of a Zig-Zag approach. The refined T32 model predicts non-conservative buckling loads and its accuracy degrades as the face-to-core thickness ratio increases. The classical FSDT is practically unable to capture the effect of the face-to-core thickness ratio and provides systematically a buckling load that is about 95% of the Euler load. From the above results, it appears that the transverse normal deformation energy does only play a marginal role for thick cores: the global buckling mode does primarily involve a transverse shear deformation of the core.

Tab. 9 refers to the Gr-Ep/foam sandwich strut with $h_f/h = 0.10$ and variable Young's modulus of the isotropic foam. Reference solutions obtained

h_f/h	0.02	0.04	0.08	0.12	0.16	0.20
Ref	0.7173	0.5692	0.4205	0.3508	0.3161	0.3018
FSDT / T32	0.7172	0.5691	0.4205	0.3509	0.3162	0.3018
CLPT / T32	0.7172	0.5691	0.4206	0.3510	0.3164	0.3022
CLPT / T30	0.7169	0.5690	0.4205	0.3510	0.3164	0.3022
CLPT / FSDT	0.7169	0.5690	0.4205	0.3510	0.3164	0.3022
T32ZZ	0.7172	0.5691	0.4205	0.3509	0.3162	0.3019
T10ZC	0.7169	0.5689	0.4204	0.3508	0.3161	0.3018
T32	0.7491	0.6149	0.5399	0.6082	0.7133	0.8016
FSDT	0.9475	0.9818	0.9483	0.9520	0.9558	0.9596

Table 8: Normalized global buckling load of the Gr-Ep/honeycomb sandwich strut.

E_{f1}/E_c	200	800	1600	2400	3200	4000
Ref	0.81	0.52	0.35	0.27	0.21	0.18
FSDT / T32	0.8158	0.5252	0.3568	0.2707	0.2183	0.1832
CLPT / T32	0.8163	0.5254	0.3569	0.2708	0.2184	0.1832
CLPT / T30	0.8161	0.5254	0.3569	0.2708	0.2184	0.1833
CLPT / FSDT	0.8161	0.5254	0.3569	0.2708	0.2184	0.1833
T32ZZ	0.8158	0.5253	0.3569	0.2708	0.2184	0.1833
T10ZC	0.8155	0.5251	0.3568	0.2707	0.2184	0.1832
T32	0.8420	0.6449	0.5518	0.5088	0.4841	0.4680
FSDT	0.9573	0.9512	0.9500	0.9496	0.9494	0.9492

Table 9: Normalized global buckling load of the Gr-Ep/foam sandwich strut ($h_f/h = 0.1$).

with an elasticity approach have been digitally extracted from the graph in [64] and have thus been reported with only 2 decimal digits. Again, accurate buckling loads are predicted for the whole range of core's moduli by LW and Zig-Zag models. Non-conservative predictions are obtained by the ESL models T32 and FSDT. The accuracy of the refined T32 model degrades with the increase of the face-to-core stiffness ratio. On the other hand, FSDT does barely sense the effect of this ratio and constantly predicts a buckling load that is only 5% less than the classical Euler load.

Wrinkling. The attention is here focused on the short-wavelength instability of compressed sandwich struts by referring to the following case study.

geometry sandwich strut with $a/h = 10$ and $h_f/h = 0.02$ ($h = 30\,mm$).

boundary conditions simple support at $x_1 = 0, a$.

materials orthotropic Graphite-Epoxy (Gr-Ep) faces: $E_{f1} = 181\,GPa, E_{f2} = E_{f3} = 10.3\,GPa, G_{f23} = 5.96\,GPa, G_{f13} = G_{f12} = 7.17\,GPa, \nu_{f23} = 0.400, \nu_{f13} = \nu_{f12} = 0.277$.

Isotropic PVC foam core: $\nu_c = 0.3$, E_c defined by the ratio $E_{f1}/E_c = 200, 800$.

results non-dimensional critical load defined in Eq. (40) as a function of h/λ, where $\lambda = a/m$ is the half-wavelength and m the number of half-waves of the periodic buckling mode along x_1.

reference values are obtained by means of a quasi-3D model [65]

Only those models that perform well in the global buckling analysis are assessed in the short wavelength wrinkling problem. Fig. 7 reports the response of the sandwich strut made out of Gr-Ep faces and an isotropic core with $E_{f1}/E_c = 200$ (left) and $E_{f1}/E_c = 800$ (right). Non-dimensional global buckling and wrinkling loads are reported in Tab. 10. The fundamental wrinkling mode of a sandwich strut with an isotropic core is known to be antisymmetric, symmetric modes are always associated to higher loads [65]. From both graphics it can be seen that all models predict accurately the global buckling load ($m = 1 \rightarrow \lambda = a = 10h$), but that their response is more disparate for shorter wavelengths, i.e., increasing h/λ ratios. Models incorporating the transverse normal deformation of the core are capable of grasping a local minimum of the response at short wavelengths, which corresponds to the wrinkling load. On the other hand, it is not possible for the models based on the plane-stress assumption to capture the wrinkling response. The

CLPT/FSDT model has not been included in Fig. 7 for it yields very similar results as CLPT/T30. A hierarchic accuracy can be appreciated: the three-layers model FSDT/T32 is indistinguishable from the reference solution up to very short wavelengths ($\lambda > h/2$); furthermore, employing CLPT instead of FSDT in the faces introduces some minor discrepancies only for $\lambda < h/3$; finally, the ESL model T32ZZ differs from the reference solution already for $\lambda < 5h$ and it predicts a non-conservative wrinkling load that is more than 30% higher than the reference value.

As a closing remark, note that the wrinkling results fully substantiate Koiter's recommendation, for they confirm that the transverse normal deformation is necessary for capturing the short wavelength response, i.e., for enhancing the accuracy of two-dimensional shell/plate models.

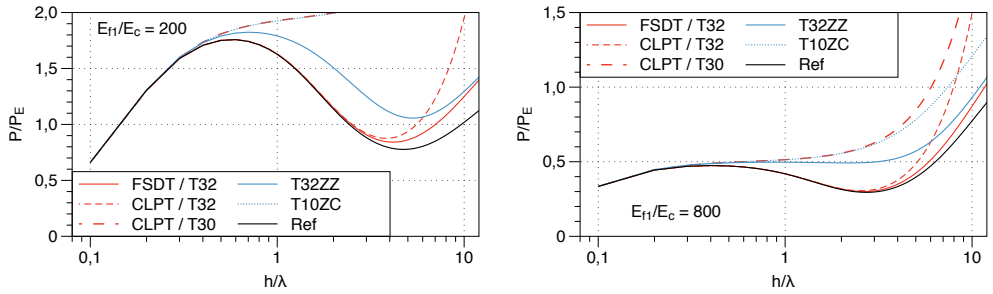

Figure 7: Non-dimensional buckling loads *vs* wavelength parameter h/λ for a Gr-Ep / foam sandwich strut ($a/h = 10$, $h_f/h = 0.02$) with $E_{f1}/E_c = 200$ and $E_{f1}/E_c = 800$.

E_{f1}/E_c	200			800		
	P_G	P_W	(m)	P_G	P_W	(m)
Ref	0.6604	0.7767	(47)	0.3344	0.2948	(27)
FSDT / T32	0.6603	0.8419	(42)	0.3344	0.3001	(26)
CLPT / T32	0.6604	0.8757	(38)	0.3344	0.3056	(25)
CLPT / T30	0.6584	–	–	0.3342	–	–
CLPT / FSDT	0.6585	–	–	0.3342	–	–
T32ZZ	0.6605	1.0564	(53)	0.3348	–	–
T10ZC	0.6584	–	–	0.3342	–	–

Table 10: Nondimensional global buckling (P_G) and wrinkling loads (P_W) of the Gr-Ep/foam sandwich strut ($a/h = 10$, $h_f/h = 0.02$). Numbers in parentheses indicate the number of half-waves m at wrinkling.

Acknowledgments

The Authors gratefully acknowledge A. Loredo and P. Vidal for their support in the numerical evaluation of exact solutions and refined Sinus-based theories.

References

[1] A. W. Leissa, Vibration of shells, Tech. Rep. NASA SP-288, NASA (1973).

[2] R. Ballarini, The Da Vinci–Euler–Bernoulli beam theory? (2003) [cited 2006].
URL `www.memagazine.org/contents/current/webonly/webex418.html`

[3] B. M. Fraeijs de Veubeke, A Course in Elasticity, Vol. 29 of Applied Mathematical Sciences, Springer Verlag New York, 1979.

[4] A. L. Gol'denveizer, Theory of Elastic Thin Shells, 2nd Edition, Pergamon Press, Oxford, 1961.

[5] A. L. Gol'denveizer, Derivation of an approximate theory of bending of a plate by the method of asymptotic integration of the equations of the theory of elasticity, J. Appl. Math. Mech. 26 (1962) 1000–1025.

[6] P. Cicala, Asymptotic approach to linear shell theory, Tech. Rep. 6, AIMETA, Italian Association of Theoretical and Applied Mechanics (1977).

[7] S. S. Antman, The theory of rods, in: C. Truesdell (Ed.), Mechanics of Solids, Vol. 2, Springer-Verlag, 1984, pp. 641–704.

[8] V. L. Berdichevsky, Variational-asymptotic method of constructing a theory of shells, P. M. M. 43 (1979) 664–687.

[9] V. L. Berdichevsky, An asymptotic theory of sandwich plates, Int. J. Eng. Sci. 48 (2010) 383–404.

[10] W. Yu, D. H. Hodges, V. V. Volovoi, Asymptotic construction of Reissner-like composite plate theory with accurate strain recovery, Int. J. Solids Struct. 39 (2002) 5185–5203.

[11] P. G. Ciarlet, P. Destuynder, A justification of the two-dimensional plate model, J. Mécanique 18 (1979) 315–344.

[12] K. Washizu, Variational Methods in Elasticity and Plasticity, 2nd Edition, Pergamon Press, 1975.

[13] E. Reissner, On a variational theorem in elasticity, J. Math. and Phys. 29 (1950) 90–95.

[14] E. Reissner, On a certain mixed variational theorem and a proposed application, Int. J. Numer. Meth. Eng. 20 (1984) 1366–1368.

[15] E. Carrera, Developments, ideas and evaluations based upon Reissner's Mixed Variational Theorem in the modeling of multilayered plates and shells, Appl. Mech. Rev. 54 (2001) 301–329.

[16] E. Carrera, Historical review of zig-zag theories for multilayered plates and shells, Appl. Mech. Rev. 56 (2003) 287–308.

[17] J. N. Reddy, Energy Principles and Variational Methods in Applied Mechanics, 2nd Edition, John Wiley & Sons, Inc., 2002.

[18] O. C. Zienkiewicz, R. L. Taylor, The Finite Element Method, 5th Edition, Vol. 1: The basis, Butterworth-Heinemann, 2000.

[19] Z. P. Bažant, L. Cedolin, Stability of Structures, Dover Publications, 2003.

[20] M. D'Ottavio, O. Polit, W. Ji, A. M. Waas, Benchmark solutions and assessment of variable kinematics models for global and local buckling of sandwich struts, Compos. Struct. 156 (2016) 125–134.

[21] A. W. Leissa, Conditions for laminated plates to remain flat under in-plane loading, Compos. Struct. 6 (1986) 261–270.

[22] R. P. Ley, W. Lin, U. Mbanefo, Facesheet wrinkling in sandwich structures, Tech. Rep. NASA/CR-1999-208994, NASA (1999).

[23] K. Niu, R. Talreja, Modeling of wrinkling in sandwich panels under compression, J. Eng. Mech. 125 (1999) 875–883.

[24] J. N. Reddy, Mechanics of Laminated Composite Plates and Shells: Theory and Analysis, 2nd Edition, CRC Press, 2004.

[25] K.-J. Bathe, Finite Element Procedures, Prentice-Hall, New Jersey, 1996.

[26] E. Reissner, The effect of transverse shear deformation on the bending of elastic plates, J. Appl. Mech. 12 (1945) A69–A77.

[27] R. D. Mindlin, Influence of rotatory inertia and shear on flexural vibrations of isotropic, elastic plates, J. Appl. Mech. 18 (1951) 31–38.

[28] J. M. Whitney, Shear correction factors for orthotropic laminates under static load, J. Appl. Mech. 40 (1973) 302–304.

[29] W. H. Wittrick, Analytical three-dimensional elasticity solutions to some plate problems and some observations on Mindlin's plate theory, Int. J. Solids Struct. 23 (1987) 441–464.

[30] V. Birman, C. W. Bert, On the choice of shear correction factor in sandwich structures, J. Sandwich Struct. Mater. 4 (2002) 83–95.

[31] W. T. Koiter, A consistent first approximation in the general theory of thin elastic shells, in: W. T. Koiter (Ed.), The Theory of Thin Elastic Shells, IUTAM, North-Holland, Delft, 1959, pp. 12–33.

[32] E. Carrera, C_z^0-Requirements - models for the two dimensional analysis of multilayered structures, Compos. Struct. 37 (1997) 373–383.

[33] K. P. Soldatos, T. Timarci, A unified formulation of laminated composite, shear deformable, five-degrees-of-freedom cylindrical shell theories, Compos. Struct. 25 (1993) 165–171.

[34] O. Polit, M. Touratier, High-order triangular sandwich plate finite element for linear and non-linear analyses, Comput. Meth. Appl. Mech. Eng. 185 (2000) 305–324.

[35] M. Touratier, An efficient standard plate theory, Int. J. Eng. Sci. 29 (1991) 901–916.

[36] S. Cheng, Elastiticity theory of plates and a refined theory, J. Appl. Mech. 46 (1979) 644–650.

[37] J. N. Reddy, A simple higher-order theory for laminated composite plates, J. Appl. Mech. 51 (1984) 745–752.

[38] A. Bhimaraddi, L. K. Stevens, A higher order theory for free vibration of orthotropic, homogeneous, and laminated rectangular plates, J. Appl. Mech. 51 (1984) 195–198.

[39] H. Murakami, Laminated composite plate theory with improved in-plane response, J. Appl. Mech. 53 (1986) 661–666.

[40] M. D'Ottavio, B. Kröplin, An extension of Reissner Mixed Variational Theorem to piezoelectric laminates, Mech. Adv. Mater. Struct. 13 (2006) 139–150.

[41] A. Robaldo, E. Carrera, Mixed finite elements for thermoelastic analysis of multilayered anisotropic plates, J. Therm. Stresses 30 (2007) 165–194.

[42] E. Carrera, On the use of Murakami's zig-zag function in the modeling of layered plates and shells, Comput. Struct. 82 (2004) 541–554.

[43] E. Carrera, S. Brischetto, Analysis of thickness locking in classical, refined and mixed multilayered plate theories, Compos. Struct. 82 (2008) 549–562.

[44] J.-C. Paumier, A. Raoult, Asymptotic consistency of the polynomial approximation in the linearized plate theory. Application to the Reissner-Mindlin model, in: ESAIM: Proceedings, Vol. 2, SMAI, 1997, pp. 203–213.

[45] S. M. Alessandrini, D. N. Arnold, R. S. Falk, A. L. Madureira, Derivation and justification of plate models by variational methods, in: M. Fortin (Ed.), Plates and Shells, Vol. 21 of CRM Proceedings and Lecture Notes, American Mathematical Society, 1999, pp. 1–20.

[46] K. H. Lo, R. M. Christensen, E. M. Wu, A high-order theory of plate deformation - Part 1: Homogeneous plates - Part 2: Laminated plates, J. Appl. Mech. 44 (1977) 663–668; 669–676.

[47] P. Vidal, O. Polit, A refined sinus plate finite element for laminated and sandwich structures under mechanical and thermomechanical loads, Comput. Meth. Appl. Mech. Eng. 253 (2013) 396–412.

[48] O. Polit, M. D'Ottavio, P. Vidal, High-order plate finite elements for smart structure analysis, Compos. Struct. 151 (2016) 81–90.

[49] J. N. Reddy, A generalization of two-dimensional theories of laminated composite plates, Comm. Appl. Numer. Meth. 3 (1987) 173–180.

[50] D. H. Robbins Jr, J. N. Reddy, Modelling of thick composites using a layerwise laminate theory, Int. J. Numer. Meth. Eng. 36 (1993) 655–677.

[51] G. M. Kulikov, S. V. Plotnikova, Exact 3D stress analysis of laminated composite plates by sampling surfaces method, Compos. Struct. 94 (2012) 3654–3663.

[52] E. Carrera, Theories and finite elements for multilayered plates and shells: A unified compact formulation with numerical assessment and benchmarking, Arch. Comput. Meth. Eng. 10 (2003) 215–296.

[53] E. Carrera, M. Cinefra, M. Petrolo, E. Zappino, Finite Element Analysis of Structures through Unified Formulation, John Wiley & Sons, Ltd, 2014.

[54] L. Demasi, ∞^3 hierarchy plate theories for thick and thin composite plates: The generalized unified formulation, Compos. Struct. 84 (2008) 256–270.

[55] L. Demasi, ∞^6 Mixed plate theories based on the generalized unified formulation. Part I: Governing equations, Compos. Struct. 87 (2009) 1–11.

[56] L. Demasi, Partially Layer Wise advanced Zig Zag and HSDT models based on the Generalized Unified Formulation, Eng. Struct. 53 (2013) 63–91.

[57] M. D'Ottavio, A Sublaminate Generalized Unified Formulation for the analysis of composite structures and its application to sandwich plates bending, Compos. Struct. 142 (2016) 187–199.

[58] A. K. Noor, W. S. Burton, Assessment of computational models for sandwich panels and shells, Comput. Meth. Appl. Mech. Eng. 124 (1995) 125–151.

[59] N. J. Pagano, Exact solutions for rectangular bidirectional composites and sandwich plates, J. Compos. Mater. 4 (1970) 20–34.

[60] O. Polit, M. Touratier, A new laminated triangular finite element assuring interface continuity for displacements and stresses, Compos. Struct. 38 (1997) 37–44.

[61] E. Carrera, C^0 Reissner-Mindlin multilayered plate elements including zig-zag and interlaminar stress continuity, Int. J. Numer. Meth. Eng. 39 (1996) 1797–1820.

[62] A. Loredo, Exact 3D solution for static and damped harmonic response of simply supported general laminates, Compos. Struct. 108 (2014) 625–634.

[63] H. G. Allen, Analysis and Design of Structural Sandwich Panels, Pergamon Press, 1969.

[64] G. A. Kardomateas, An elasticity solution for the global buckling of sandwich beams/wide panels with orthotropic phases, J. Appl. Mech. 77 (2010) 021015.1–7.

[65] M. D'Ottavio, O. Polit, Linearized global and local buckling analysis of sandwich struts with a refined quasi-3D model, Acta Mech. 226 (2015) 81–101.

[66] S. P. Timoshenko, J. M. Gere, Theory of Elastic Stability, McGraw-Hill, New York, 1961.

[67] V. Z. Vlasov, Thin-Walled Elastic Beams, 2nd Edition, Israel Program for Scientific Translations Ltd., 1963.

[68] P. Ladevèze, J. Simmonds, New concepts for linear beam theory with arbitrary geometry and loading, Eur. J. Mech. Solids 17 (1998) 377–402.

[69] R. El Fatmi, Non-uniform warping including the effects of torsion and shear forces. Part I: A general beam theory, Int. J. Solids Struct. 44 (2007) 5912–5929.

[70] V. Giavotto, M. Borri, P. Mantegazza, G. Ghiringhelli, V. Carmaschi, G. C. Maffioli, F. Mussi, Anisotropic beam theory and applications, Comput. Struct. 16 (1983) 403–413.

[71] D. H. Hodges, Nonlinear composite beam theory, AIAA, Inc., 2006.

[72] V. L. Berdichevsky, On the energy of an elastic rod, J. Appl. Math. Mech. 45 (1981) 518–529.

[73] A. R. Atilgan, D. H. Hodges, Unified nonlinear analysis for nonhomogeneous anisotropic beams with closed cross sections, AIAA J. 29 (1991) 1990–1999.

[74] W. Yu, D. H. Hodges, Generalized Timoshenko theory of the variational asymptotic beam sectional analysis, J. Am. Helicopter Soc. 50 (2005) 46–55.

[75] W. Yu, D. H. Hodges, J. C. Ho, Variational asymptotic beam sectional analysis - An updated version, Int. J. Eng. Sci. 59 (2012) 40–64.

[76] P. Vidal, O. Polit, A sine finite element using a zig-zag function for the analysis of laminated composite beams, Compos. B 42 (2011) 1671–1682.

[77] P. Vidal, O. Polit, A family of sinus finite elements for the analysis of rectangular laminated beams, Compos. Struct. 84 (2008) 56–72.

[78] P. Vidal, O. Polit, Assessment of the refined sinus model for the nonlinear analysis of composite beams, Compos. Struct. 87 (2009) 370–381.

[79] P. Vidal, O. Polit, A refined sine-based finite element with transverse normal deformation for the analysis of laminated beams under thermomechanical loads, J. Mech. Mater. Struct. 4 (2009) 1127–1155.

[80] E. Carrera, G. Giunta, M. Petrolo, Beam Structures - Classical and Advanced Theories, John Wiley & Sons, Ltd, 2011.

Appendix A. Beam models

Beam structures[1] are slender bodies that are loaded in the most general, three-dimensional, case by axial and shear forces as well as bending and torsion moments. As outlined in Section 1, a beam model is formulated by taking advantage of the slenderness and it consists of (*i*) a closed set of PDE or ODE that depends on only one independent variable (the coordinate along the beam axis); (*ii*) the definition of the stiffnesses of the cross-sectional surface, which in turn depend on the geometric and material properties; (*iii*) some relations for recovering the stress state in any point of the body from the solution of the one-dimensional problem. The key point is thus to define the cross-sectional deformation, generally referred to as *warping*, and various approaches have been followed for accomplishing this task.

The classical axiomatic approach is referred to as the Saint-Venant theory: based on static assumptions (stresses perpendicular to the beam axis are nil), it considers a cross-section that remains plane when the beam is loaded by axial force and bending moments, but that is free to warp uniformly out of its plane under the action of a torsion moment and shearing forces. In-plane warping is included in Saint-Venant's theory through the Poisson effect. Classical beam theories such as Euler-Bernoulli's or Timoshenko's are formulated within the framework of Saint-Venant's approach upon introducing further restrictive assumptions that limit the out-of-plane warping to torsional deformation: a rigid cross-section is thus postulated for the extension, bending and - within Timoshenko's theory - shearing, while uniform Saint-Venant's warping is retained for torsion.

Refined models that go beyond Saint-Venant's theory are required in presence of non-uniform (restrained) warping [67], which typically occurs in thin-walled beams, or whenever a short wavelength response is to be evaluated [68, 69]. Furthermore, composite cross-sections require high-order warping functions for including the elastic couplings between extension, bending, shearing and torsion, which are of utmost importance in a number of specific and complex applications such as beam models for helicopter rotor blades. In this context, it is worth mentioning the early work by Giavotto *et al*

[1]Following Antman [7], such structural members are also called "rods". "Column" or "truss" most often indicate a beam that is subjected to only axial loads, the latter term being preferred for geometrically linear formulations. So, "beam-columns" indicate one-dimensional structures subjected to axial and lateral loads simultaneously [66].

[70], in which Saint-Venant's theory was enriched through warping functions obtained from a cross-sectional finite-element analysis, as well as the unified, nonlinear approach of Hodges and coworkers summarized in [71]. The framework of this latter approach is Berdichevsky's Variational-Asymptotic Method [72], which allows to formulate one-dimensional beam models with high-order warping functions and whose accuracy is defined in an asymptotic sense, see also [73–75].

The remainder of this Appendix will limit the attention to composite beam models without considering torsion, i.e., for which out-of-plane warping may be induced under bending load due to the transverse shear flexibility of the composite cross-section. For the sake of conciseness, complicating effects such as taper ratio, initial twist and curvature, and thin-walled open cross-sections will be left out of the scope.

Straight prismatic beams are considered that occupy the volume $V = \mathcal{S} \times [0, L]$, where L is the length of the beam measured along the x_1 axis and $\mathcal{S}$ is the cross-section in the (x_2, x_3)-plane. Let further the cross-section $\mathcal{S}$ be rectangular of dimension $b \times h$ and composed of N_p plies, where $h = \sum_{p=1}^{N_p} h^{(p)}$ is the thickness measured along the $x_3 = z$ coordinate and b is the width measured along the $x_2 = y$ coordinate. The procedure for constructing the reduced one-dimensional model starting from the elasticity relations can be still formally introduced as in Section 2, but the two-dimensional domain Ω has to be replaced by the one-dimensional domain $x_1 \in \{0, L\}$ and the thickness direction z by the two-dimensional cross-section $(y, z) \in \mathcal{S}$. The kinematic approximations are thus introduced into Hamilton's principle as

$$u_i(x_1, x_2, x_3; t) = F_{s_i}(y, z)\tilde{u}_{s_i}(x_1; t) \qquad \text{with } s_i = 0, 1, 2, \dots N_i \qquad \text{(A-1)}$$

and the differentiations and integrations of Eq. (9) can be explicitly carried out over $\mathcal{S}$.

Appendix A.1. Classical theories

Classical theories rely on the hypothesis of an infinitely rigid cross-section thus decoupling bending and torsion. In analogy to the CLPT and FSDT theories for plates, one discerns the Euler-Bernoulli Beam Theory (EBBT) and the Timoshenko Beam Theory (TBT) that are next described.

Euler-Bernoulli Beam Theory. The EBBT can be formulated according to following kinematic assumption:

1. *the cross-section is infinitely rigid in its plane.*
2. *the cross-section remains plane and perpendicular to the beam axis during deformation.*

The first assumption states that no stress nor deformation exist in the cross-sectional $(y, z)-$plane, that is, a one-dimensional constitutive relation is used for relating the axial strain and the axial stress. The planarity of the cross-section enforces a linear distribution of the displacement field across $\mathcal{S}$, i.e., the displacement field is constructed as a superposition of an axial displacement and a rigid rotation of $\mathcal{S}$. The perpendicularity condition states the equivalence between the rotations of the cross-section and the slope of the deformed beam axis, which means that the transverse shear strains γ_{xy} and γ_{xz} are nil. One notices the correspondence with the CLPT discussed in Section 3.1 and illustrated in Fig. 2(b). The displacement field for the EBBT thus reads

$$u_1(x_1, y, z; t) = \tilde{u}_{0_1}(x_1; t) - y\,\frac{\partial \tilde{u}_{0_2}(x_1; t)}{\partial x_1} - z\,\frac{\partial \tilde{u}_{0_3}(x_1; t)}{\partial x_1} \tag{A-2a}$$

$$u_2(x_1, y, z; t) = \tilde{u}_{0_2}(x_1; t); \qquad u_3(x_1, y, z; t) = \tilde{u}_{0_3}(x_1; t) \tag{A-2b}$$

Note that only 3 unknown functions suffice to express the EBBT kinematics, which correspond to the displacement vector $[\tilde{u}_{0_1},\, \tilde{u}_{0_2},\, \tilde{u}_{0_3}]$ of a generic point of the beam axis x_1.

Timoshenko Beam Theory. TBT extends EBBT upon introducing a transverse shear strain field that is constant across $\mathcal{S}$, and it relies on following kinematic assumptions:

1. *the cross-section is infinitely rigid in its plane.*
2. *the cross-section remains plane during deformation.*

Based on these assumptions, the displacement field for the TBT in the three-dimensional space can be written as

$$u_1(x_1, y, z; t) = \tilde{u}_{0_1}(x_1; t) + y\,\tilde{u}_{1_1}(x_1; t) + z\,\tilde{u}_{2_1}(x_1; t) \tag{A-3a}$$

$$u_2(x_1, y, z; t) = \tilde{u}_{0_2}(x_1; t); \qquad u_3(x_1, y, z; t) = \tilde{u}_{0_3}(x_1; t) \tag{A-3b}$$

The 5 unknown functions that define the TBT kinematics are thus the displacement vector $\tilde{u}_{0_i}$ of a point on the beam axis and the rotations $\tilde{u}_{1_1}$ and $\tilde{u}_{2_1}$ about the z and y axes, respectively, of the rigid cross-section. Note the correspondence with the FSDT discussed in Section 3.2 and illustrated in Fig. 2(c). Shear correction coefficients can be included for reducing the transverse shear deformation energy predicted by the uniform transverse shear stresses of TBT.

Appendix A.2. Refined theories

Refinements to the previously outlined classical theories are formulated upon relaxing the assumption of a rigid cross-section, i.e., including a warping deformation that - in the present context that neglects torsion - is due to transverse shear strains. In the following and in view of the numerical assessment proposed in Appendix A.3, the discussion shall be limited to refined theories formulated within the framework of the Sinus-model. The HSDT kinematics reads

$$u_1(x_1,y,z;t) = \tilde{u}_{0_1}(x_1;t) - y\,\frac{\partial \tilde{u}_{0_2}(x_1;t)}{\partial x_1} + f(y)\left(\tilde{u}_{1_1}(x_1;t) + \frac{\partial \tilde{u}_{0_2}(x_1;t)}{\partial x_1}\right) - z\,\frac{\partial \tilde{u}_{0_3}(x_1;t)}{\partial x_1} + f(z)\left(\tilde{u}_{2_1}(x_1;t) + \frac{\partial \tilde{u}_{0_3}(x_1;t)}{\partial x_1}\right) \tag{A-4a}$$

$$u_2(x_1,y,z;t) = \tilde{u}_{0_2}(x_1;t); \qquad u_3(x_1,y,z;t) = \tilde{u}_{0_3}(x_1;t) \tag{A-4b}$$

where one retrieves EBBT and TBT by setting $f(y) = f(z) = 0$ and $f(y) = y,\ f(z) = z$, respectively, while for a Sinus-theory one sets

$$f(y) = \frac{h}{\pi}\sin\left(\frac{\pi y}{b}\right); \qquad f(z) = \frac{h}{\pi}\sin\left(\frac{\pi z}{h}\right) \tag{A-5}$$

In case of beam problems defined in the $(x_1, z)-$plane, the kinematics Eq. (A-4) reduces simply to

$$u_1(x_1,y,z;t) = \tilde{u}_{0_1}(x_1;t) - z\,\frac{\partial \tilde{u}_{0_3}(x_1;t)}{\partial x_1} + f(z)\left(\tilde{u}_{2_1}(x_1;t) + \frac{\partial \tilde{u}_{0_3}(x_1;t)}{\partial x_1}\right) \tag{A-6a}$$

$$u_3(x_1,y,z;t) = \tilde{u}_{0_3}(x_1;t) \tag{A-6b}$$

Zig-Zag theories can be formulated which account for the slope discontinuity of the axial displacement u_1 along the stacking direction $x_3 = z$. For this, one may directly superimpose Murakami's Zig-Zag Function (MZZF) defined in Eq. (33) to the HSDT kinematics, see [76]; alternatively, the slope discontinuity is introduced by fulfilling the Interlaminar Continuity of the transverse shear stress - see the AMT approach outlined in Section 4.2 and the formulation presented in [77, 78]. One may note that the dependence on the $x_2 = y$ coordinate remains unaffected in either case because the plies are assumed to be stacked along $x_3 = z$ only.

All theories mentioned above retain the static assumption of Saint-Venant's theory, which calls for the use of the one-dimensional constitutive law for plane stress. The full three-dimensional constitutive law can be employed

upon retaining the direct stresses in the cross-sectional plane and following the same arguments outlined in Section 4.3. In the case of a plane problem, the HSDT of Eq. (A-6) can be enhanced with a quadratic expansion for the transverse displacement as follows [79]

$$u_1(x_1, y, z; t) = \tilde{u}_{0_1}(x_1; t) - z\,\frac{\partial \tilde{u}_{0_3}(x_1; t)}{\partial x_1} + f(z)\left(\tilde{u}_{2_1}(x_1; t) + \frac{\partial \tilde{u}_{0_3}(x_1; t)}{\partial x_1}\right) \tag{A-7a}$$

$$u_3(x_1, y, z; t) = \tilde{u}_{0_3}(x_1; t) + z\,\tilde{u}_{1_3}(x_1; t) + z^2\,\tilde{u}_{2_3}(x_1; t) \tag{A-7b}$$

All beam theories discussed above have a number of unknown functions that is independent of the number of plies constituting the composite cross-section. Refined Layer-Wise beam models are obtained in the very same manner as mentioned in Section 5 and lead to models with a number of unknown functions and, hence, DOF that depends on the number of the considered layers.

Carrera's Unified Formulation (CUF) permits to build classical and refined beam models, based on ESL or LW descriptions, in the same way as outlined in Section 6 by directly employing the generic expansion given in Eq. (A-1): the cross-section $\mathcal{S}$ is discretized in a number $\tau = 1, 2, \dots N$ of points that are interpolated by a given polynomial basis $F_\tau(y, z)$ (Taylor, Lagrange, Legendre, ...), and the solution of each point u_τ is only dependent on the axial coordinate, i.e., $u_\tau = u_\tau(x_1)$. The interested reader may consult [80], a book entirely dedicated to the description of Carrera's Unified Formulation for beam structures. It is emphasized that CUF can be effectively employed for determining, in a combined axiomatic-asymptotic sense, the "best" model for a given application, i.e., the model of lowest order that provides with a predefined accuracy a specific result for a specific problem. The specific result may be related to global or local response, and the specific problem is defined by geometry, material, boundary and loading conditions.

Appendix A.3. Assessment on some benchmark problems

The same benchmark configurations addressed for the assessment of plate models in Section 7 are here employed to assess several classical and refined ESL theories based on the Sinus model. The different models are identified following the same naming convention summarized in Tab. 1. The proposed assessment concerns the effect of the length-to-thickness ratio $S = a/h$ for straight beam problems in the $(x_1, z)-$plane. Non-dimensional fundamental frequencies for the simply-supported non-symmetric 2-ply and symmetric 3-ply laminated beams are displayed in Tab. A.11. The non-dimensional

static response of simply-supported beams subjected to the sinusoidal load $p_3(x_1, z = \frac{h}{2}) = p_0 \sin \frac{\pi x_1}{a}$ are given in Tab. A.12 for the 2-ply laminate and in Tab. A.13 for the 3-ply laminate. The reported non-dimensional quantities are defined according to Eq. (37). Results for simply-supported sandwich beams are displayed in Tab. A.14 (non-dimensional fundamental frequencies defined by Eq. (38)) and Tab. A.15 (static response defined according to Eq. (37a)).

	2 plies $(0°, 90°)$			3 plies $(0°, 90°, 0°)$		
S	4	10	100	4	10	100
Ref	4.5105	5.7700	6.1672	5.8545	10.334	13.930
S2ZC	4.5525	5.7827	6.1673	5.8569	10.335	13.931
S2	4.6390	5.8104	6.1712	6.0488	10.599	13.940
S0ZC	4.8284	5.8580	6.1682	5.9758	10.345	13.930
S0Z	4.6169	5.8029	6.1676	5.9660	10.417	13.932
S0	4.7040	5.8254	6.1678	6.0502	10.629	13.939
FSDT	4.6784	5.8254	6.1678	6.8997	11.418	13.955
CLPT	5.9253	6.1305	6.1712	13.644	13.933	13.989

Table A.11: First natural frequency of simply-supported cross-ply laminated beams.

It is apparent that the comments made in Section 7 for the plate problem assessments are valid for the considered plane beam problems as well. Classical theories (EBBT, TBT) can be employed for thin beams ($S = 100$), for all models yields very similar results in this case. When dealing with moderately thick ($S = 10$) and thick ($S = 4$) beams, the results show that the most accurate model is S2ZC: on the one hand, the Zig-Zag effect is required for capturing the effects introduced by the layers' interfaces within the composite stack, on the other hand, the three-dimensional constitutive law should be retained for including the transverse normal deformation energy, which is no longer negligible when the beam is thick ($S = 4$). These conclusions demonstrate once again the validity of Koiter's recommendation [31] (see Section 4) in the case of composite structures.

z	$-\bar{U}_1$ (h/2)	$\bar{U}_3$ (0)	$-\bar{\sigma}_{11}$ (-h/2)	$\bar{\sigma}_{13}$ (max)
S=4				
Ref	0.0714	4.7081	1.8762	0.6764
S2ZC	0.0720	4.6231	1.9367	0.6371
S2	0.0546	4.2833	1.8087	0.5838
S0ZC	0.0544	4.1878	2.0958	0.4193
S0Z	0.0722	4.5438	1.9903	0.6918
S0	0.0613	4.4027	2.1200	0.6297
FSDT	0.0603	4.4347	1.7496	0.4547
S=10				
Ref	0.0623	2.9611	1.7652	0.7230
S2ZC	0.0623	2.9481	1.7750	0.6687
S2	0.0582	2.8445	1.7450	0.6021
S0ZC	0.0593	2.8836	1.8068	0.4331
S0Z	0.0623	2.9374	1.7872	0.7039
S0	0.0604	2.9156	1.8101	0.6426
FSDT	0.0603	2.6254	1.7496	0.4547
S=100				
Ref	0.0603	2.6288	1.7443	0.7337
S2ZC	0.0602	2.6160	1.7373	0.6763
S2	0.0601	2.6173	1.7413	1.5774
S0ZC	0.0603	2.6280	1.7502	0.4358
S0Z	0.0603	2.6285	1.7500	0.7064
S0	0.0603	2.6283	1.7502	0.6451
FSDT	0.0603	2.6283	1.7496	0.4547
CLPT	0.0603	2.6255	1.7496	-

Table A.12: Bending of the simply-supported $(0°, 90°)$ beam under sinusoidal load.

model z	$-\bar{U}_1$ (h/2)	$\bar{U}_3$ (0)	$-\bar{\sigma}_{11}$ (-h/2)	$\bar{\sigma}_{13}$ (0)
S=4				
Ref	0.0148	2.8901	1.1304	0.3580
S2ZC	0.0146	2.8913	1.1871	0.3545
S2	0.0135	2.6853	1.0974	0.2950
S0ZC	0.0158	2.7916	1.2469	0.3855
S0Z	0.0155	2.8027	1.2224	0.3363
S0	0.0139	2.7258	1.0974	0.2904
FSDT	0.0080	2.0941	0.6324	0.1592
S=10				
Ref	0.0094	0.9332	0.7361	0.4239
S2ZC	0.0093	0.9331	0.7374	0.4336
S2	0.0090	0.8719	0.7250	0.3254
S0ZC	0.0095	0.9321	0.7459	0.4450
S0Z	0.0095	0.9193	0.7519	0.4043
S0	0.0090	0.8828	0.7105	0.3048
FSDT	0.0080	0.7642	0.6324	0.1592
S=100				
Ref	0.0080	0.5153	0.6315	0.4421
S2ZC	0.0080	0.5128	0.6289	0.4556
S2	0.0080	0.5131	0.6317	0.4497
S0ZC	0.0080	0.5153	0.6335	0.4583
S0Z	0.0080	0.5151	0.6336	0.4225
S0	0.0080	0.5147	0.6331	0.3076
FSDT	0.0078	0.5135	0.6324	0.1561
CLPT	0.0080	0.5109	0.6324	-

Table A.13: Bending of the simply-supported $(0°, 90°, 0°)$ beam under sinusoidal load.

S	4	10	100
Ref	7.6880	15.677	25.335
S2ZC	7.9322	16.022	25.358
S2	8.0566	16.201	25.368
S0ZC	7.7196	15.702	25.336
S0Z	7.9807	16.074	25.351
S0	8.0750	16.240	25.359
FSDT	11.133	19.656	25.458
CLPT	24.292	25.333	25.545

Table A.14: First natural frequency of the simply-supported sandwich beam.

z	$\bar{U}_1$ (-h/2)	$\bar{U}_3$ (0)	$\bar{\sigma}_{11}$ (h/2)	$\bar{\sigma}_{13}$ (0)
S=4				
Ref	0.0299	11.061	2.3841	0.3392
S2ZC	0.0288	10.408	2.2999	0.4153
S2	0.0276	10.067	2.2263	0.4064
S0ZC	0.0305	11.028	2.3995	0.3655
S0Z	0.0297	10.315	2.3384	0.4094
S0	0.0276	10.076	2.1730	0.3942
FSDT	0.0158	5.2869	1.2476	0.1290
S=10				
Ref	0.0182	2.6688	1.4317	0.3504
S2ZC	0.0180	2.5563	1.4186	0.4286
S2	0.0176	2.4785	1.4075	0.4192
S0ZC	0.0182	2.6621	1.4378	0.3771
S0Z	0.0182	2.5397	1.4282	0.4218
S0	0.0178	2.4878	1.3986	0.4020
FSDT	0.0158	1.6927	1.2476	0.1291
S=100				
Ref	0.0159	1.0248	1.2456	0.3526
S2ZC	0.0158	1.0229	1.2465	0.4312
S2	0.0158	1.0201	1.2478	0.5062
S0ZC	0.0159	1.0247	1.2496	0.3794
S0Z	0.0159	1.0235	1.2465	0.4243
S0	0.0159	1.0229	1.2492	0.4035
FSDT	0.0158	1.0149	1.2476	0.1291
CLPT	0.0158	1.0081	1.2476	-

Table A.15: Bending of the simply-supported sandwich beam under sinusoidal load.